UNIVERSITÄT OSNABRÜCK

Influence of stochastic power generation and network heterogeneities on power grid stability

Master thesis
of
Matthias Wolff
29.9.2016

Supervisor
Prof. Dr. P. Maaß
Advisor
Dr. P. Lind

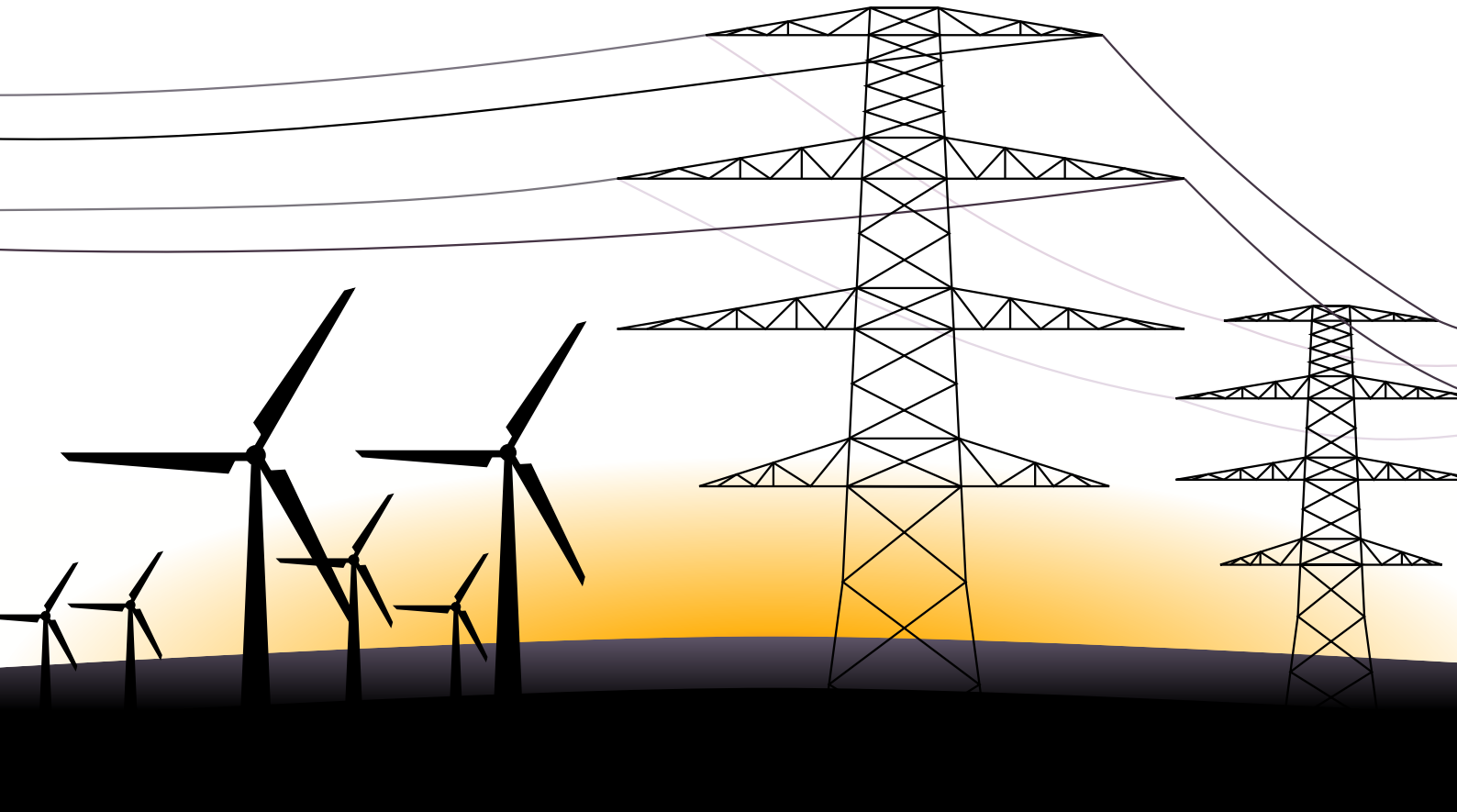

Contents

Frequently used symbols
(alphabetically ordered)

A	Scaled Power	Q	Imaginary part of power/reactive power
$\mathcal{A}$	Adjacence matrix	R	Resistance
B	Susceptance	S	Complex power
C	Connection matrix	$\mathcal{S}_\mathrm{B}$	Basin stability measure
D	Damping ratio	t	Time
d	Node degree	V	Voltage
E	Voltage of internal node	X	Reactance
G	Conductance	x_d	Transient reactance
H	Scaled inertia	Y	Admittance
I	Current	Z	Impedance
J	Inertia	ζ	Transformer phase shift
i	Imaginary unit or index	θ	Phase angle
j	index	ϕ	Admittance angle
K	Coupling strength/matrix	χ	Identifier function
M	Torque	ω	Angular velocity/frequency
N_x	Number of x	ω_r	Reference frequency (of the grid)
P	Real part of power/active power	$()^*$	Complex conjugate

Used short cuts
(alphabetically ordered)

BS	Basin stability (measure)
EN	Effective Network (model)
ER	Erdös-Rényi (network)
FP	Fixed Point
IC	Initial Conditions
KMO	Kuramoto Oscillators
PF	Power-Flow (equation)
SM	Synchronous Machines (model)
SP	Structure Preserving (model)
VL	Voltage Level (of transmission grid)

1. Motivation, Structure and Introduction

A stable and reliable electrical power supply is an essential component of the prosperity of the modern society. The production of almost every good is fully or partial reliant on electrical energy. Together with the industry and the medical supply a huge part of our living standards depends on electricity. Not only every private household but also all telecommunication systems, the media, both also of great relevance at the political level, as well as computer-technology that changed the conditions of industry production, and scientific research depends to a large extent on energy supply.

Energy, and in particular electricity, is provided[1] by power grids, that connect the set of power plants within a country or continent with the consumers ans loads. Power plants are the generators and provide electrical power. The reason of using electrical power instead of other sources is that it can be produced centralized and transported easily. This transport (or distribution) is done through transmission lines that together with generators and loads compose the power grid.

Not all consumers are equal. Households use a voltage of $230V$ (in Germany), industry higher voltages ($10\text{k}V$-$100\text{k}V$) and the long transmission lines even higher voltages at $200kV$ to $400kV$. Hence the transmission grid has different voltage levels for every specific task. The interaction between all these components is mediated through equations based on graph theory. In the context of graph theory the consumers and generators are the nodes of the graph and the transmission lines are the edges among them, see Figure 2.1.

In the optimal case the power grid works in the so-called steady state, in other words all generators (and consumers depending on the modelling) work at the reference frequency of the grid, which in Germany is 50Hz. Furthermore all voltages must be constant or near that. To determine the steady state of a grid the so called Power-Flow (PF) equations are used [2]. If the grid gets perturbed, when for example a transmission line gets broken, some of the conditions of the PF equations are violated and the grid is no longer in the steady state and the changes in the phase angles of the nodes is described by the swing equation [2]. One important question that rises in this context is whether the grid returns to the steady state or not? To answer this question is the aim of this thesis. The ability of the power grid to return to the steady state after being perturbed depends on the grids properties as well as on the nature of the perturbation.

Thereby two kinds of perturbations are analysed. One with instantly changing phase angle and angular velocity and another with continuous power fluctuations. The second is of special interest in Germany since the energy production in this country should be

[1] In this work by (electrical) power or energy production is meant the conversion from for instance mechanical power or energy to electrical. It is assumed - as usual in physics - that energy cannot be created or annihilated.

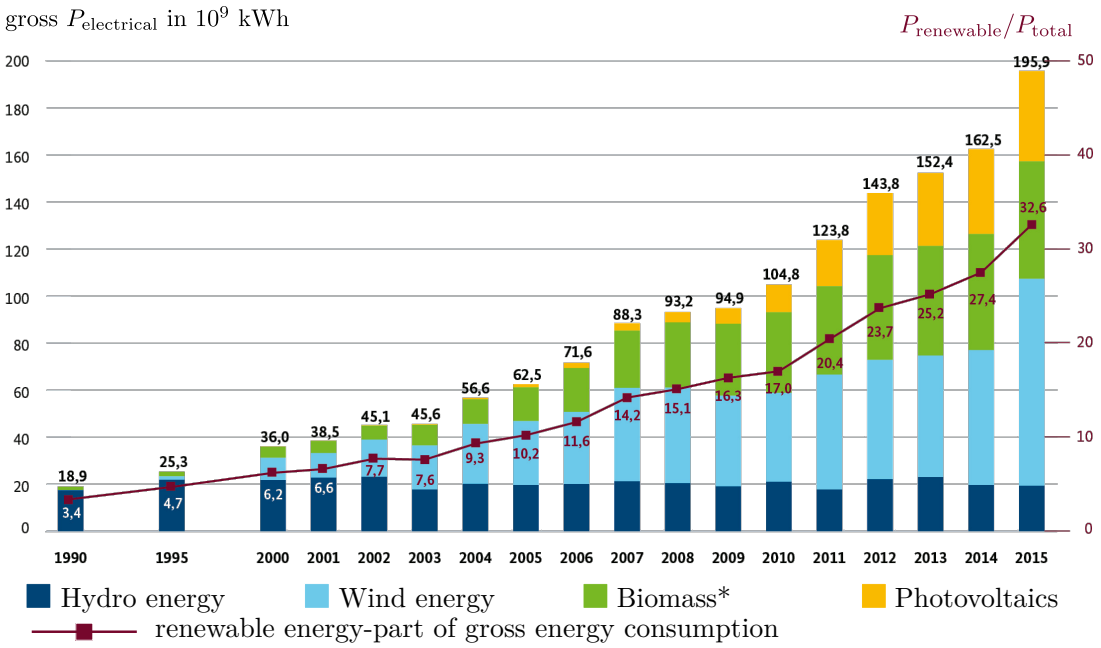

Geothermic energy is not shown due to the small amount of energy.

*Including solid and liquid biomass, biogas, biomethan, sewage- and landfill gas and biogenic part of waste, from 2013 also sewage sludge

Figure 1.1.: Progress of the energy produced by renewable energy sources in Germany since 1990 [1]. The bars show the gross electrical energy production in billion kilo-watt-hours and their partitioning to the different energy sources. The dark red line shows the percentage of the renewable energy on the gross energy consumption.

more and more provided by *renewable* energy sources due to ecological and political reasons as well as a lack of fossil resources, see Figure 1.1. One of the most important renewable energy sources is the wind power as shown in Figure 1.2. Since it fluctuating on different time scales it is important to investigate its influence on the power grid stability.

One important feature that should be taken into account when designing a power grid is the heterogeneity of the components. Since transmission lines have to be installed in diverse geographical regions, like small villages on mountains or densely populated urban areas their capacities vary strongly. This is reflected by a large heterogeneity in the admittances of the lines. Therefore we expect a difference in the grids stability when modelling the transmission lines identical (homogeneous network) or with different admittances (heterogeneous network). Results of this investigation are given in this thesis that emphasis the use of heterogeneous networks.

In Chapter 2 the basics of power grid modelling are described. Important concepts are explained as the synchronous machine and transmission lines and a brief introduction

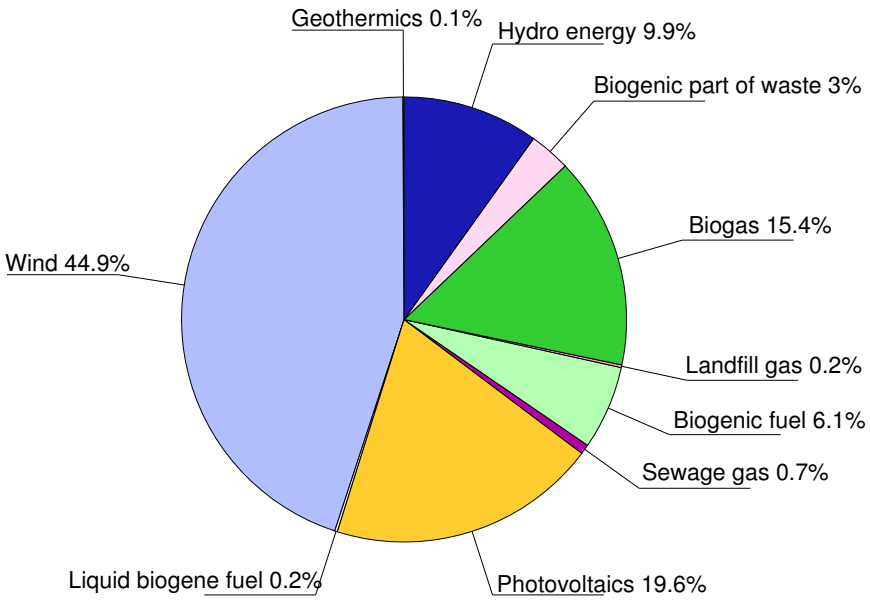

Figure 1.2.: Detailed partitioning of the 195.9 billion kWh produced by renewable energy sources in Germany in 2015 [1].

in graph theory is given. On that basis we will start with an investigation of a single generator connected to an effective infinite grid in Chapter 3. Thereupon the model is extended to multiple generators and consumers and their interaction in Chapter 4. Thereby the power grid will be simplified with homogeneous quantities for generators, consumers and transmission lines to investigate the topology and introduce important methods and properties of power grids. In Chapter 5 the models are applied to power grids whose properties are available in public. Since these grids contain parameters that do not occur in our equations the transformation of these values to model-parameters is discussed. Finally a conclusion and an outlook is given.

2. Modelling of power grids

A common way to approach on power grids is describing them as networks. The power *generators* which are usually power plants and *consumers* that could be for example cities or industrial areas are the *nodes* of the network, see figure 2.1. They are connected by *edges* between them that are transmission lines. These exist in different voltage levels that come along with diverse network structures.

In the next section 2.1 we will address the voltage levels and elucidate which level our modelling fits. A short general introduction into networks is given in Section 2.2 in which the terms nodes, edges and adjacency matrix are specified. Furthermore different transmission line models are discussed in Section 2.3 and in more detail later in Section 5.1 because a detailed treatment of them is not necessary in the first chapters.

The nodes of the network represent synchronous machines. As the name suggest, their behaviour is related to the term *synchronization* which is closely linked to the *Kuramoto-Model* which is the topic of Section 2.4. Then the synchronous machines are described in Section 2.5 physically. For the mathematically description the *Power-Flow equations* are needed that are derived in Section 2.6. Then the dynamic behaviour of the synchronous machines is addressed in Section 2.7.

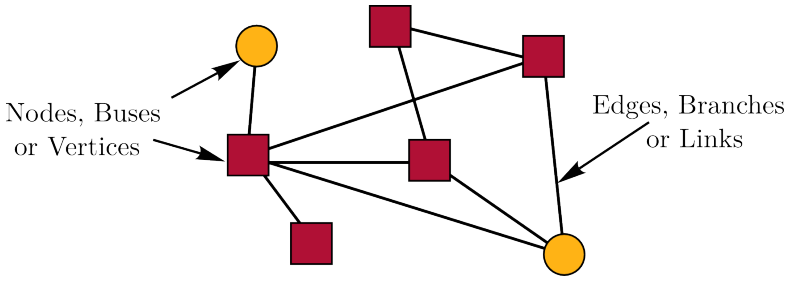

Figure 2.1.: An example of an undirected network.

2.1. Voltage Levels in the Transmission Grid

Transmission grids are divided into four different voltage levels (VL) each one with a particular task. Depending on the country in which the grid is located there might be differences. The existing levels are listed in table 2.1. The table and the following presentation is related to the german transmission grid as explained for instance in [3].

The highest-VL contains only generators as nodes and transmission lines that work at 220 kV to 400 kV. This lines are used for energy transport over long distances up to

Level	Voltage	Purpose
Highest-voltage	380 kV/400 kV	energy transport over long distances (up to 1000 km) with little losses
	220 kV	older versions of the highest-voltage transmission grid
High-voltage	110 kV	distribution and supply for large industrial complexes
Medium-voltage	10-20 kV	distribution on smaller scales (<1 km) and industrial supply
Low-voltage	220-380 V	supply for private households and companies with little energy consumption

Table 2.1.: Voltage levels of the german power grid with corresponding purposes.

1000 km. The losses are minimized because of the high voltage and thus low current for the same power. Consequently these transmission lines allow a centralized electric energy generation. Large power plants with more than one gigawatt can be used to cover the energy demand of a wide area of consumers. One advantage of this kind of power plant is that they are able to produce power more efficiently and less costly than smaller ones.

The next lower VL is about 100 kV. This voltage still allows an energy transport over distances of the magnitude of kilometers. At this level first consumers appear namely industrial complexes that have a high energy demand for instance large electric motors. On the other hand industrial complexes that produce power can inject it to this stage of the grid while this mostly happens at medium-VL.

The medium-VL ranges from 1 kV to 30 kV and mainly distributes electric power in cites or country sides. It is also usual that smaller power plants ($\leq$300 MW) and private or industrial energy producers feed in electric energy to this level.

Finally the low-VL supplies households and firms with little energy consumption.

In this work we will only model the high-voltage transmission grid. The generation and consumption of a region is gathered to one node each. As a first approximation the transformers and electrical substations can be reduced [4] in the sense of *Kron reduction* that will be explained in detail in Section 5.2.

2.2. Network Representation

One of the biggest and most famous networks is the internet (world wide web), where the nodes are routers and the edges are ip-address-links. Other examples are streets or power grids which will be investigated in this thesis.

There are lots of different classifications of networks according to the properties of their components. For example a network can be *undirected*, if every edge can be used

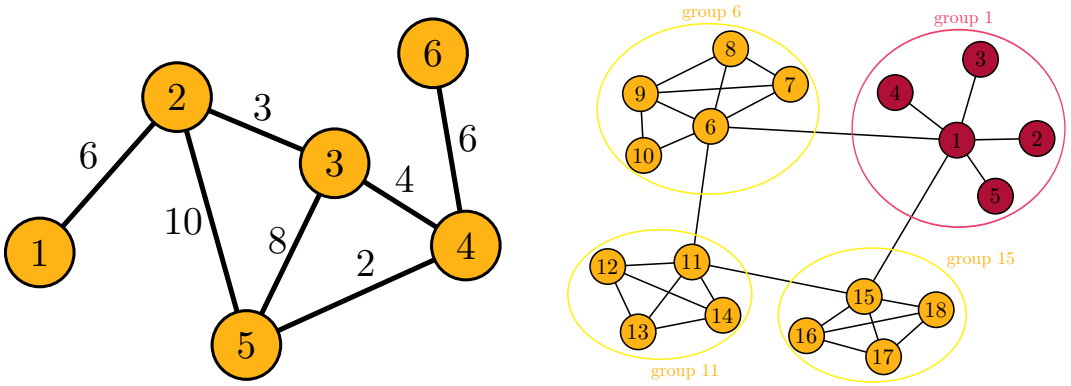

(a) (b)

Figure 2.2.: (a) Example network for illustration of shortest path length. The numbers near to the edges indicate their connection strength. (b) Example network with three high clustered groups (6, 11 and 15) and one unclustered group (1).

to get from its first connected node to the second and backwards, like normal streets, or *directed* like one way streets. If all edges have the same strength the network is called *unweighted* otherwise it's called *weighted*. Power grids are typically weighted networks which can be directed or undirected depending of the modelling of the branches.

The mathematical base to describe phenomena in networks is the Graph Theory introduced by Leonhard Euler in 1736. Here a very brief introduction to Graph Theory is given which only focusses on the topics that are important in this work.

The central concept of graph theory is the adjacency matrix $\mathcal{A}$ whose components a_{ij} are one if node i is connected to node j and zero otherwise. When referred to the adjacency matrix its often spoken of the *topology* of the graph or of the network. If the network is undirected the adjacency matrix is symmetric $a_{ij} = a_{ji}$. Often when dealing with weighted networks the components of the adjacency matrix are multiplied with the connection strength k_{ij} of the corresponding edge. Here we will call this matrix K with $K_{ij} = k_{ij}a_{ij}$ the *coupling matrix* what will become clear, see Chapter 2.4.

With the introduction of the adjacency matrix, quantities that come along with networks and their characterization can be derived. Of particular interest are the shortest path between to nodes and the clustering coefficient.

The former can easily be understood as follows. We consider the network shown in Figure 2.2(a). The shortest path between two nodes, say 1 and 5, is calculated as follows. There are three possibilities to reach node 5 from node 1 (without going in loops), for example $1 \to 2 \to 5$. If the network is unweighted this would be the shortest path $l^{\mathrm{uw}}_{1,5}$, since it contains the less possible edges, as summarized in Table 2.2. But in the weighted case the weight of every edge must be added up therefore the shortest path $l^{\mathrm{w}}_{1,5}$ is $1 \to 2 \to 3 \to 4 \to 5$ with (weighted) length 15. The *average* shortest path length $\langle l \rangle$ is obtained by calculating the (weighted or unweighted) shortest path length for every

pair (i, j) and average them over all $N_\mathrm{n}(N_\mathrm{n}-1)/2$ pairs in the undirected or $N_\mathrm{n}(N_\mathrm{n}-1)$ pairs in the directed case. For an undirected network it is obtained by

$$\langle l \rangle = \frac{2}{N_\mathrm{n}(N_\mathrm{n}-1)} \sum_i \sum_j l_{ij}^{\mathrm{w/uw}} \ . \tag{2.1}$$

The *clustering coefficient* c can be explained as a measure how probable two nodes are connected when they are both connected to a third node. The network in Figure 2.2(b) for instance has three groups that are strongly connected (clustered) and one weakly clustered. Imagine that the nodes represent persons and the edges if the persons know each other, the resulting network is often called a *social network*. In such networks usually *cliques* occur which can be understood as in the common language a circle (cluster) of friends. Their characteristic are a large number of connections within the group and few connections to other groups.

The clustering coefficient c_i of a node i consequently indicates the number of connections N_c of the g_i neighbours of i in relation to the possible number of connections $g_i(g_i-1)/2$ between them. Mathematically we can express this behaviour by

$$c_i = \frac{2N_\mathrm{c}}{g_i(g_i-1)} = \frac{\sum_{j,n} a_{ij}a_{jn}a_{ni}}{g_i(g_i-1)} \, , \tag{2.2}$$

in the case of an undirected and unweighted network.

We will use these concepts when we create random networks in Section 4.1. Going into more detail would bring us beyond the scope of this work. For further literature see [5] or [6].

path	$l_{\mathrm{uw},1,5}$	$l_{\mathrm{w},1,5}$
$1 \to 2 \to 5$	2	16
$1 \to 2 \to 3 \to 5$	3	17
$1 \to 2 \to 3 \to 4 \to 5$	4	15

Table 2.2.: All possible paths (without loops) between node 1 and 5 in Figure 2.2(a) and their unweighted and weighted length.

2.3. Transmission Line Model - the Edges of the Network

Transmission lines are principally wires connecting power plants, consumers and transformation stations. There are three usual ways to describe them mathematically depending on their properties such as the length. The simplest way is to model them as impedances, see Figure 2.3(a). In Chapters 3 and 4 we will use this model since we start with studies of the power grid model and the topology and in Chapter 5 consider more realistic networks.

The admittance matrix Y is obtained by multiplying the components a_{ij} of the adjacency matrix $\mathcal{A}$ with the admittance $y_{ij} = 1/Z_{ij}$ of the corresponding line $Y_{ij} = y_{ij}a_{ij}$. The coupling matrix K is in the special case of the node modelling used in the following chapters (before Chapter 5) obtained by multiplying the voltage of the connected nodes (i and j) with the admittance and qualitatively equal to it $Y \propto K$. A more general valid derivation is given in Section 5.3.

A representation of transmission lines often used in simulations including all important properties of the lines [7] is shown in Figure 2.3(b). A transformer that is called *tap transformer* with *tap ratio* τ is connected in series with an impedance Z which is therefore called *series impedance* Z_S. Also two condensers are connected in parallel with the susceptance B that is called *line charging susceptance*. In this case the transmission lines and hence the admittance (and also adjacency and coupling) matrix is not symmetric. A detailed explanation of this model is given in Section 5.1.

Since most of the transmission lines does not have such a tap transformer the modelling for these lines is identical to the *π-model* shown in Figure 2.3(c). The name

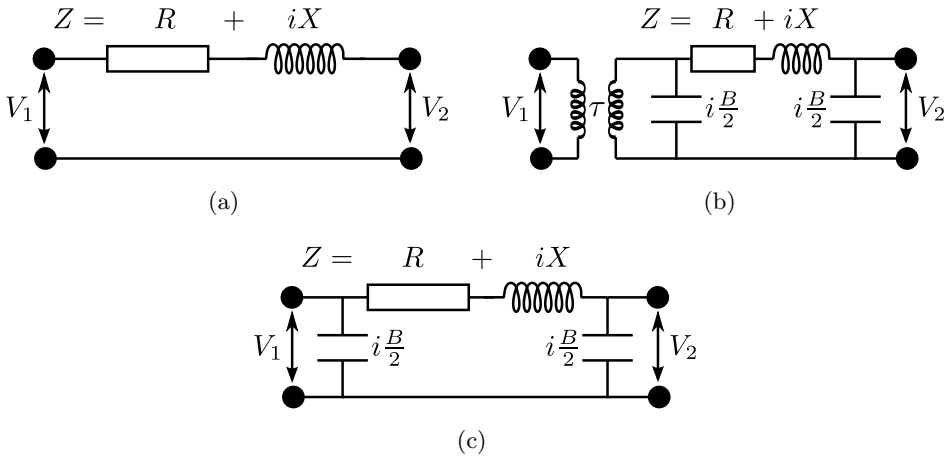

Figure 2.3.: Usual models for transmission lines connecting to nodes 1 and 2 with voltages V_1 and V_2. (a) Simplest model where the transmission line only consists of an impedance $Z = R+iX$. (b) A line consists of an impedance Z, two condensers connected in parallel and a transformer in series marked with τ. (c) As (b) without the transformer. Since most lines does not have such a transformer this model affect most of the lines.

originates from the fact that the condensers and the impedance together are shaped like a π.

2.4. Synchronization and Kuramoto-Model

As the name synchronous machine suggests that will be investigated in the following sections, the synchronization phenomenon is an important feature of the stability of a power grid. The term synchronization originates from the Greek language with σύν "syn" for together and $\chi\rho\acute{o}\nu o\zeta$ "chronos" for time. The meaning is the equalization of the phase- /angular velocities of oscillating objects due to their (weak) interaction. The oscillating objects are self excited in this case, in other words they are driven by an internal energy source to keep their inherent frequency when not coupled to other ones. A synchronous generator for instance compensates its damping losses by burning fuel (if its a conventional generator). Other examples are the clapping of an audience or the lighting of Lampyridaes (Fireflies).

If we observe an oscillator in a co-rotating frame which rotates with the inherent frequency of the oscillator its phase θ is arbitrary but fixed. It can be shifted by small perturbations or influences. This is important for the synchronization process since they are coupled by their phases.

A basic model to investigate synchronization phenomena due to phase coupling was developed by Yoshiki Kuramoto [8] and is hence called *Kuramoto-Model*. It consists of N coupled phase oscillators (or Kuramoto-oscillator KMO in the following) with inherent frequency ω_i whose dynamic is governed by

$$\frac{\mathrm{d}\theta_i}{\mathrm{d}t} = \omega_i + \frac{K}{N}\sum_{j=1}^{N}\sin(\theta_j - \theta_i), \tag{2.3}$$

where K is the coupling strength equal for every oscillator. This implies that every KMO is coupled to any other resulting in an undirected, homogeneous weighted and fully connected network. In the thermodynamic limit $N \to \infty$ this is called mean-field case. The inherent frequencies are drawn from a given probability distribution $g(\omega)$ which is a (Cauchy-)Lorentz distribution in the original work. Here, for all simulations we use

$$g(\omega) = \frac{1}{\pi}\frac{s}{s^2 + (\omega - \omega_0)^2}, \tag{2.4}$$

with $s = 0.5$ and $\omega_0 = 0$.

To analyse the synchronicity Kuramoto defined an order parameter, namely

$$re^{i\Psi} = \frac{1}{N}\sum_{j=1}^{N} e^{i\theta_j}, \tag{2.5}$$

with i the imaginary unit. If all phase angles (θ_j) are equal, r is one and it means all KMOs are fully synchronized, they have the same phase angle, as illustrated in Figure 2.4 on the right hand side. This occurs for a coupling strength $K \to \infty$.

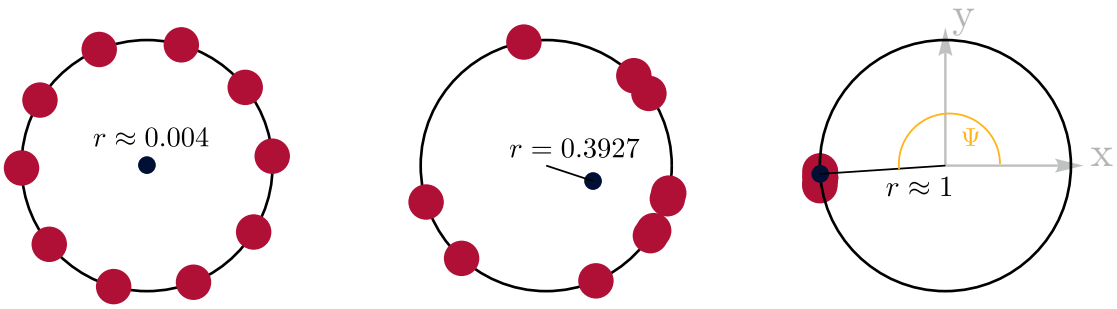

Figure 2.4.: Illustration of the Kuramoto-oscillators as red spheres. They are located at (x = cos(θ),y = sin(θ)) so their phase determines the position on the black circle with $R = 1$. The small black dot represents the order parameter and can be seen as the "mass centre" of the oscillators. Its distance from the centre of the black circle is equal to the order parameter r and its angle (to the x-axis) is Ψ. The figure on the right hand side shows fully synchronized oscillators, the middle figure partially synchronized ones and the left figure desynchronized ones. These figures show one moment in time. While the phase angle difference for synchronized oscillators is constant it changes over time for other ones as described in the text.

Notice that parameter $r = r(t)$ is dependent on time since the system synchronizes not instantly, as shown in Figure 2.5. Therefore the important measure is the r_∞ the order parameter converges to. At a arbitrary time t, $r(t)$ could be greater than zero but if the system does not synchronize then in time average r_∞ is zero. This average case for desynchronized oscillators is shown in the left sketch of Figure 2.4 and appears for a coupling constant lower than a threshold K_c.

In other words we can denote that for $K > K_c$ the order parameter r converges to a constant over time t since the angular velocities of the synchronized oscillators are equalized. The fluctuation arises from the other oscillators with arbitrary angular velocity and therefore a permanently changing phase angle relation. Synchronicity means equal angular velocities. The coupling constants $K_c < K$ "$< \infty$" lead to a partial synchronized system. The dependence $r_\infty(K)$ is plotted in Figure 2.6.

The critical value K_c, equal to one in this case, is dependent on the distribution of in inherent frequencies $g(\omega)$ and can be calculated in the mean field case [9], yielding

$$K_c = \frac{2}{\pi\, g(0)} \,. \tag{2.6}$$

With this value it is possible to obtain the (mean field) dependence $r(K)$ analytically that reads

$$r(K) = \sqrt{1 - \frac{K_c}{K}}\,, \quad K \geq 1. \tag{2.7}$$

The Kuramoto-model with a finite number of oscillators shows a partial synchronicity $r > 0$ for $K < K_c$ that vanishes with increasing N.

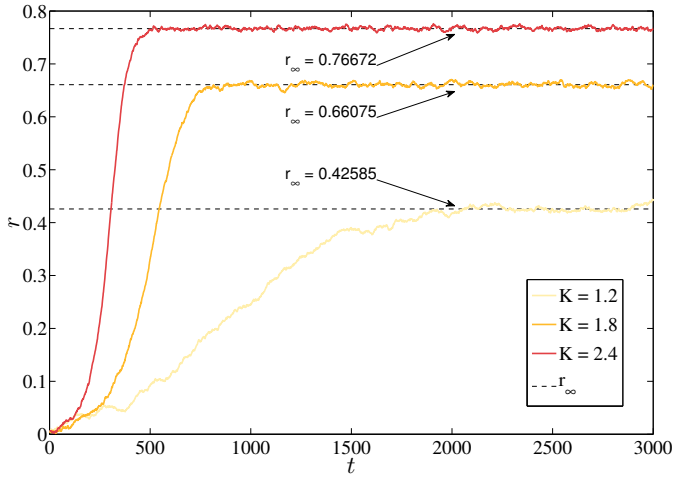

Figure 2.5.: Order parameter r over time t for different coupling constants K and $N = 10000$. The dashed lines show the values r_∞.

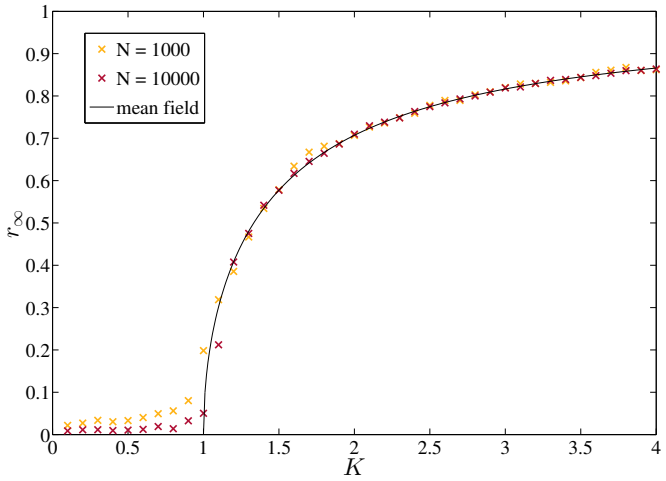

Figure 2.6.: Convergence value r_∞ of r versus the coupling constant K. Simulation results (crosses) with finite numbers of oscillators are compared to mean field case with $N \to \infty$. The transition $r_\infty > 0$ at K_c is smooth for finite oscillators.

The Kuramoto-Model can be extended in many different ways. The swing equation, that is addressed in the next section, is equivalent to a model with an additional inertia term $J\frac{\mathrm{d}^2\theta}{\mathrm{d}t^2}$. Therefore this approach is often called "second order Kuramoto-model approach of power grid modelling".

2.5. Synchronous Machines - the nodes of the network

Generators in power grids are always realized as synchronous machines which are advantageous as they run with the same frequency as the network once synchronization is reached. This guarantees a maximum possible power transmission. The functionality of a synchronous machine, that can be used as generator or motor is discussed in this section without describing it mathematically while the important equations are addressed in the next Section 2.7.

A sketch of such a generator (or motor) is shown in Figure 2.7. It consists on an *stator* that is spatially fixed and contains the *stator windings* that are separated into three groups (U, V and W) since in power grids a three-phase current is used [3]. These voltages (or currents) in these wires are 120° phase shifted against each other as explained later. The other major component is the *rotor* which is mounted in a way that it can rotate around its y-axis, as shown in Figure 2.7, but fixed in the other directions. In the rotor there are embedded *excitation windings* with a direct current flowing through them which creates a magnetic field whose magnitude is constant in time. Alternatively permanent magnets can be used instead of the excitation windings.

The number of poles of the excitation windings is denoted by p. They occur always in pairs since one, or maybe a group of them, (two in Figure 2.7), comprise a current flowing in +y direction and another a current in -y direction. This results in p magnetic poles.

When operating as a generator the rotor is driven by an external force, for instance a turbine. Hence the magnetic field moves with the same angular velocity as the rotor. This spatially rotating magnetic field induces an alternating voltage in the stator windings. The number of oscillations of the magnetic field over the whole circle of the stator is equal to the number of pole pairs (which is $\frac{p}{2}$) and also equal to the number of stator windings of each type U, V and W, see Figure 2.8. The magnitude of the magnetic field at for example the two U-windings (U_1 and U_2) is identical. Therefore the three stator windings can be connected in series or parallel respectively and the voltages adds up. This is also valid for the V and W windings.

The idea of using more than one dipole is in reducing the rate of rotation because one oscillation in the magnetic field also means one oscillation in the induced alternating voltage and hence a higher frequency relative to the rotor. The relation between the rotor speed ω_{rot} and the voltage frequency ω_{V} reads

$$\omega_{\mathrm{V}} = \frac{p}{2}\omega_{\mathrm{rot}} \ . \tag{2.8}$$

For example hydroelectric plants use a pole pair number of 30 and more ($p = 60$)

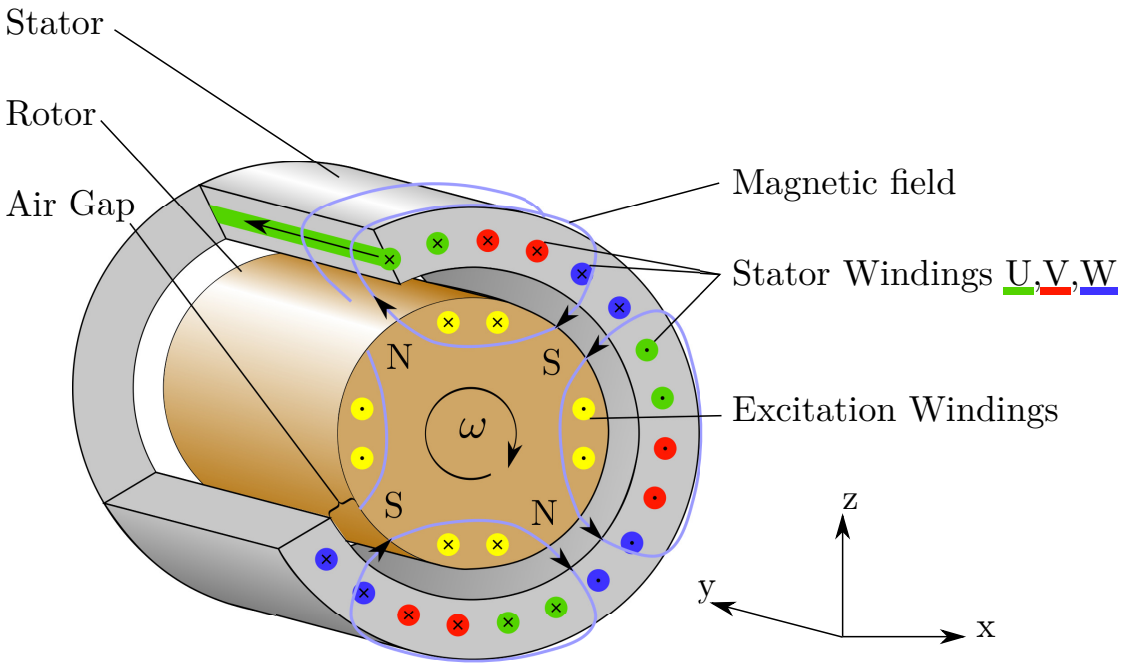

Figure 2.7.: Illustration of a synchronous generator, in this special case a four pole generator since it has four groups of excitation windings (yellow) and therefore four magnetic poles, marked with N for north-pole and S for south-pole. Also the stator windings occur twice each. The excitation windings are embedded into the rotor that can rotate around its y-axis. Hence the magnetic field (light blue), induced by a direct current flowing through the excitation windings, also rotates with the same speed. The direction of the current is marked by a cross for +y direction and a dot for -y direction. The movement of the magnetic field induces an alternating voltage in the stator windings (red, green and blue for each of the three phases respectively).

since the water turbines can not rotate as fast as gas turbines.

In the following we will treat every synchronous machine in the investigated power grid as an one pole pair machine since we only need ω_V to describe the synchronization phenomenon and can treat the rotation of the rotor as an effective one.

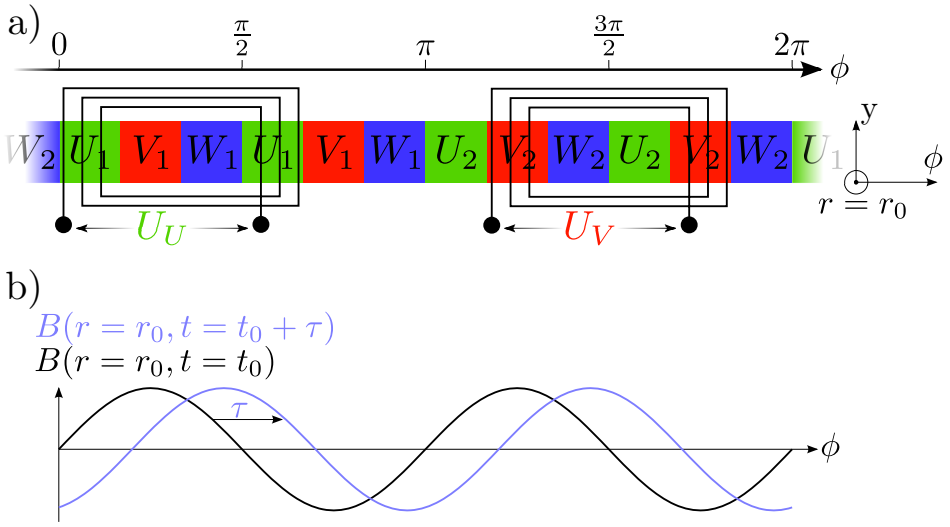

Figure 2.8.: a) The synchronous generator illustrated in cylindrical coordinates or in other words the cylinder containing all stator windings unrolled to a plane. The winding are located at radius $r = r_0$ from the centre of the generator, see Figure 2.7. b) The magnitude of the magnetic field induced by the excitation windings at the radius r_0 for two different times t_0 and $t_0 + \tau$.

2.6. Power-Flow Equations - the Steady State

A power grid is in a steady state, if all phase-angle-differences θ_j at each node j are constant as well as all currents I_j and voltages V_j. That implies that the power requested by the loads is provided by the generators. Furthermore all frequencies are equal to the reference frequency ω_r of the grid therefore $\omega = 0$ in the co-rotating frame rotating with ω_r. The question of how to determine this state is answered in this section.

In power grid analysis usually one make use of the calculation with power instead of calculating with currents and voltages as usual for passive electrical circuits. This eases the calculation of the dynamic case and also the parametrization of the generators.

The complex power values are denoted by

$$S_j = P_j + iQ_j = V_j I_j^* \tag{2.9}$$

for all nodes ($j = 1, 2, ..., N_\mathrm{n}$) with the currents

$$I_j = \sum_{k=1}^{N_\mathrm{n}} Y_{jk} V_k \tag{2.10}$$

where Y is the Y_0-matrix derived in the Section 2.3 and in more detail in Section 5.1. The quantities I and V are thereby complex. Hence the voltage $V = |V|e^{i\theta}$ has a phase

	Variable	Known values	Unknown values
	P	N_n	0
	Q	N_c	N_g
	θ	1	$N_\mathrm{n} - 1$
	V	N_g	N_c
total	-	$2N_\mathrm{n} + 1$	$2N_\mathrm{n} - 1$

Table 2.3.: List of variables needed to solve PF equation and quantity of given values and unknowns. The number of generators in the grid is N_g, the number of consumers is N_c and $N_\mathrm{n} = N_\mathrm{g} + N_\mathrm{c}$ is the number of all nodes.

θ. Equation (2.10) inserted in equation (2.9) yields

$$S_j = \sum_{k=1}^{N_\mathrm{n}} |V_j||V_k| \left[G_{jk} \cos\left(\theta_j - \theta_k\right) + iB_{jk} \sin\left(\theta_j - \theta_k\right)\right] \quad \text{or} \tag{2.11a}$$

$$S_j = \sum_{k=1}^{N_\mathrm{n}} |V_j||V_k||Y_{jk}| \exp\left(i\left(\theta_j - \theta_k - \phi_{jk}\right)\right) \tag{2.11b}$$

with the conductance $G = \mathrm{Re}(Y)$, the susceptance $B = \mathrm{Im}(Y)$ and the phase angle $\phi_{jk} = \arctan\left(B_{jk}/G_{jk}\right)$.

The complex power can be divided into the active power P and the reactive power Q. That leads to a non-linear equation system

$$P_j = \sum_{k=1}^{N_\mathrm{n}} |V_j V_k Y_{jk}| \cos\left(\theta_j - \theta_k - \phi_{j,k}\right) \tag{2.12a}$$

$$Q_j = -\sum_{k=1}^{N_\mathrm{n}} |V_j V_k Y_{jk}| \sin\left(\theta_j - \theta_k - \phi_{j,k}\right) \tag{2.12b}$$

which is called *AC Power-Flow Equations*. Usually P and V are given for generators. These are so called PV-nodes. For loads P and Q are given (PQ-nodes). We can choose one phase angle $\theta = 0$ as reference because only phase angle differences occur in the formula. So we have in summary $2N_\mathrm{n} - 1$ unknowns and $2N_\mathrm{n}$ equations, as shown in Table 2.3.

In real power grids often the phase-angle differences are held near zero for maximum power transmission. Therefore the equations can be approximated in these cases by $\sin(\Delta\theta) \approx \Delta\theta$ and $\cos(\Delta\theta) \approx 1$. The resulting equations are called *DC Power-Flow Equations*. They are a linear equation system and can be solved through e.g. gauss elimination and has one solution since it is overdetermined as listed in Table 2.3.

The AC Power-Flow (PF) equations must be solved with numerical methods like Newton-Raphson iteration.

With the toolbox MATPOWER [7] it is possible to solve both PF equation systems.

2.7. Swing Equation - the Dynamic Case

After considering the functionality of a synchronous machine in Section 2.5 here its dynamic, or more precisely the dynamic of the rotor, is investigated. For the derivation consider a turbine providing mechanical power P_m (or a mechanical torque M_m) connected to the rotor. The induction of a voltage in the stator windings results in another torque M_e which points in the opposite direction. With the rotors inertia J and a damping $\tilde{D}$ the equation of motion for the phase angle θ' reads

$$J\frac{\mathrm{d}^2\theta'}{\mathrm{d}t^2} + \tilde{D}\frac{\mathrm{d}\theta'}{\mathrm{d}t} = M_m - M_e \ . \tag{2.13}$$

The rotor is in the steady state when $\frac{\mathrm{d}\theta'}{\mathrm{d}t} = \omega = \omega_\mathrm{r}$ and the important variable is the difference of the frequency to it $\omega = \omega' - \omega_\mathrm{r}$. Considering the respective derivatives we obtain

$$\frac{\mathrm{d}\theta}{\mathrm{d}t} = \frac{\mathrm{d}\theta'}{\mathrm{d}t} - \omega_\mathrm{r}, \tag{2.14a}$$

$$\frac{\mathrm{d}^2\theta}{\mathrm{d}t^2} = \frac{\mathrm{d}^2\theta'}{\mathrm{d}t^2} \ . \tag{2.14b}$$

Equation (2.14b) the inertia term is the same in the stationary and in the co-rotating frame. Equation (2.14a) extends the damping term to $\tilde{D}\left(\frac{\mathrm{d}\theta}{\mathrm{d}t} + \omega_\mathrm{r}\right)$.

In the steady state $\left(\frac{\mathrm{d}\theta}{\mathrm{d}t} = 0\right)$ the mechanical torque M_m compensates both the electrical torque and the damping $\tilde{D}\omega_\mathrm{r}$. We will therefore introduce $\tilde{M}_m = M_m - \tilde{D}\omega_\mathrm{r}$.

As discussed before we want to express the generation and consumption by power $P = M\omega$ since torque is an inconvenient quantity. The equation can be rewritten as

$$J\omega_\mathrm{r}\frac{\mathrm{d}^2\theta}{\mathrm{d}t^2} + \tilde{D}\omega_\mathrm{r}\frac{\mathrm{d}\theta}{\mathrm{d}t} = \frac{\omega_\mathrm{r}}{\omega}\left(\omega\tilde{M}_m - \omega M_e\right) \ . \tag{2.15}$$

The fluctuation of the frequency ω usually only differs marginally from the reference frequency ω_r with $\Delta\omega = \omega - \omega_\mathrm{r} \ll 1\%$ [2], [10], and thus $\omega_\mathrm{r}/\omega \approx 1$, yielding

$$J\omega_\mathrm{r}\frac{\mathrm{d}^2\theta}{\mathrm{d}t^2} + \tilde{D}\omega_\mathrm{r}\frac{\mathrm{d}\theta}{\mathrm{d}t} = P'_m - P'_e \ . \tag{2.16}$$

All quantities are typically expressed in multiples of a base power P_R. This unit system is called the per unit (p.u.) system. Moreover, to be consistent with [2] a scaled inertia $H = \frac{1}{2}J\omega_\mathrm{r}^2/P_\mathrm{R} \Leftrightarrow 2H/\omega_\mathrm{r} = J\omega_\mathrm{r}/P_\mathrm{R}$ and $D = \tilde{D}\omega_\mathrm{r}/P_\mathrm{R}$ is used, yielding

$$\frac{2H}{\omega_\mathrm{r}}\frac{\mathrm{d}^2\theta}{\mathrm{d}t^2} = -D\frac{\mathrm{d}\theta}{\mathrm{d}t} + P_m - P_e, \tag{2.17}$$

where $P = P'/P_\mathrm{R}$. Equation (2.17) describes the dynamics of one rotor given an electrical power demand P_e. As mentioned above P_e results from the loads of the network, and

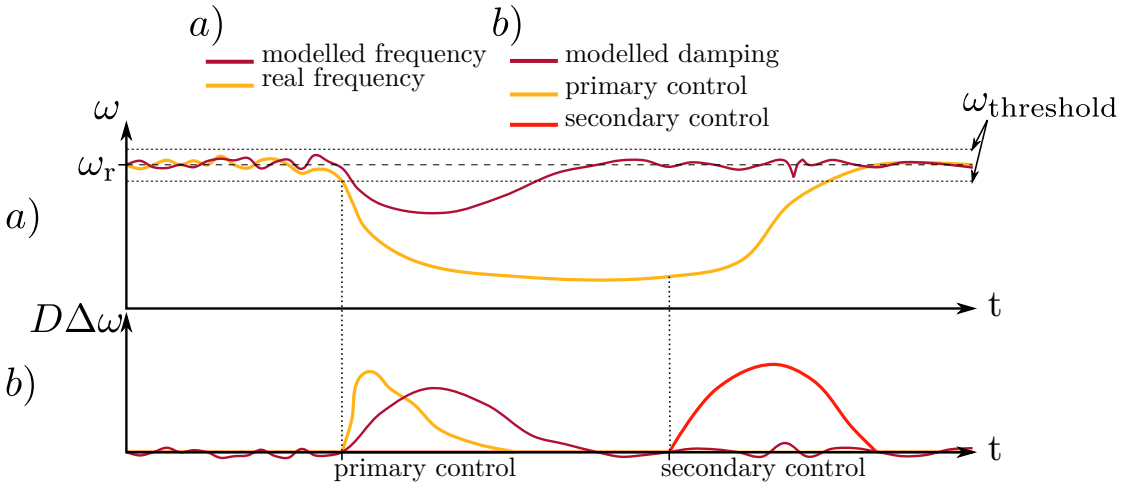

Figure 2.9.: Illustration of the damping mechanisms of power grids namely the primary and the secondary control in comparision to the modelling as permanent force. The units are arbitrary; the difference between the model and the controlling might be smaller.

therefore the interaction between the synchronous machines (and loads if not modelled as such), must be inserted into the rotors dynamic. This is done by expressing P_e through the Power Flow equation (Equation (2.12a)) investigated in Section 2.6, with the resulting flow yielding the power demand at each node. The final equation is called *swing equation* and reads

$$\frac{2H_i}{\omega_\mathrm{r}} \frac{\mathrm{d}^2\theta_i}{\mathrm{d}t^2} = -D_i \frac{\mathrm{d}\theta_i}{\mathrm{d}t} + P_{m,i} - \sum_j K_{ij} \cos\left(\theta_i - \theta_j\right) \ . \tag{2.18}$$

In this thesis we will consider Equation (2.18) to each node of the power grid.

The damping must be addressed more detailed. It consists of three parts namely the electrical damping of the windings, the mechanical damping and the regulation of the power plant governor. The electrical and mechanical damping can typically be neglected [2], [11]. The regulation of the governor is divided into different mechanisms on corresponding timescales [10].

The *primary control* is an automatic reaction on a frequency drop or rise. It reacts when frequency fluctuations exceed a threshold, as illustrated in Figure 2.9. It can be modelled as a permanent force. This mechanism is implemented in such a way, that all generators in a network are regulated simultaneously. For instance, if the frequency drops below the threshold, which means a lack of power somewhere in the system occurred, all generators of the power grid increase their power production until the drop of the frequency stops. This is of cause limited by the maximum reserve of power production. Normally it is constructed such that if any one of the power plants shuts down, the reserve of all others can compensate the power lack. The primary control operates on

timescales below one minute.

If a change in the frequency occurs then after around one minute the *secondary control* drives the frequency back to the reference frequency. This is mostly done automatically by recalculating the power production of every generator. If such control is not successful to maintain the synchronous frequency, human interaction comes to play. Here the damping is as a permanent force driving back the frequency to the reference mixing up the mechanisms of the primary and secondary control. It is identical for every node $D_i = D$.

2.8. Model and Parameter Summary

In this chapter we revisited the important concepts for describing and analysing power grids. It was demonstrated that it is possible to translate them as networks containing nodes that represent synchronous generators or motors and edges representing transmission lines. The nodes follow the swing equation, Equation (2.18). If the grid is synchronized (the relative motion of all rotors is zero, $\omega = 0$) terms containing time derivatives of the phase angle disappear and the Power-Flow equations remain with the real part given by Equation (2.12a). In both of these equations the coupling matrix K (or admittance matrix Y) occurs that mediates the interaction between the synchronous machines. It is derived from the adjacency matrix and the weights of every transmission line that is the admittance in the simplest case. An extended model is elucidated in Section 5.1. The needed parameters for the simulation of the network are given in Table 2.4.

Nodes		Branches	
P	active power	R	resistance
Q	reactive power	X	reactance
V	voltage	$Y = (R + iX)^{-1}$	admittance
D	damping ratio	$\mathcal{A}_{ij}$	adjacency to others
H	inertia (scaled)	K	coupling strength
θ_{SS}	phase angle in steady state		(derived from $\mathcal{A}$, Y and V)

Table 2.4.: Summary of the parameters used for power grid modelling in the next chapters.

3. Single node model

To get familiar with the basin stability approach and general methodology of power grid modelling we first revisit the work by Menck et al. [4] in this chapter.

In a power grid with N_n nodes the phase space compound by phases θ_j and frequencies ω_j $(i = 1, 2, ..., N_\mathrm{n})$ has dimension $2N_\mathrm{n}$. The single node model considers one node alone connected to a larger grid. In this way, one is able to investigate the influence of parameters in evolution of the phase and frequency of one node, see figure 3.1.

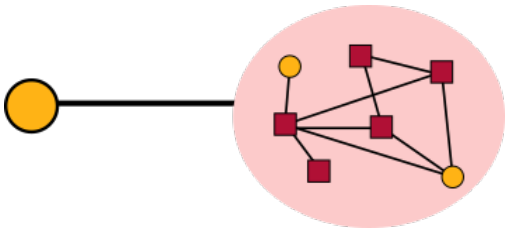

Figure 3.1.: Sketch of the single node model. The grid is assumed to be a node with is unaffected by perturbations of the single node.

We first address the mathematical background and the idea of how random initial conditions (IC) of (θ, ω) are related to single node perturbations is introduced. In section 3.2 an insight into the basin stability approach is provided that will be also used in chapter 4 for analysing the behaviour of multiple nodes in different topologies. In the end of this chapter a more detailed model of the perturbations is introduced, particularly when wind power fluctuations take place, as it is the case when wind turbines or farms are connected to the power grid.

3.1. Mathematical background

Having a single node connected to the grid, we take the grid as a second node assuming it has a constant phase angle $\dot{\theta}_\mathrm{grid} = 0$. This model is also called infinite grid model in the dissertation of Menck [12].

Consequently the swing equation is reduced to

$$\dot{\omega} = -D\omega + P - K \sin\left(\theta - \theta_\mathrm{grid}\right), \tag{3.1}$$

$$\dot{\theta} = \omega, \tag{3.2}$$

$$\dot{\theta}_\mathrm{grid} = 0\ . \tag{3.3}$$

We choose $\theta_{\text{grid}} = 0$ as the reference angle [4] and thus the power flow equation reads

$$0 = P - K \sin(\theta) \tag{3.4}$$

with the stationary solutions (SS)

$$\omega_{\text{SS}}^{(1)} = 0, \tag{3.5a}$$
$$\theta_{\text{SS}}^{(1)} = \arcsin\left(\frac{P}{K}\right) \tag{3.5b}$$

and

$$\theta_{\text{SS}}^{(2)}(t) = \int_0^t \omega(t')\ \mathrm{d}t', \tag{3.6}$$
$$\omega_{\text{SS}}^{(2)}(t) \approx \frac{P}{D} + \frac{DK}{P}\cos\left(\frac{P}{D}t\right)\ . \tag{3.7}$$

The first solution only exists if $P < K$ and is called a *fixed point*. The second solution implies a frequency which is not constant and the assumption $|P|/D^2 \gg 1$, $|P|^2/D^2 \gg K$ [4] and is called *limit cycle*.

If we start a trajectory which arbitrary IC there are two attractors, one for each solution. After a sufficiently long time, the trajectory will follow the limit cycle or return to the fixed point

Lets imagine the following scenario.

The generator runs synchronously with the grid at $\omega = 0$ and $\theta = \theta_{\text{SS}}^{(1)}$. A violent storm causes the breakdown of the transmission line connecting the single node to the grid. Consequently K becomes zero and the power produced by the generator cannot be transferred to the consumer. A fraction of the power dissipates but most of it increases the rotational speed of the turbine. After some time the angular velocity and the phase angle are far away from the fix point, at $(\theta_{\text{pert}}, \omega_{\text{pert}})$, see figure 3.2(a).

When the transmission line finally gets fixed we have a situation as described above. The generators phase angle and velocity are at the IC$(\theta_{\text{pert}}, \omega_{\text{pert}})$ and the trajectory will run either to the fixed point or to the limit cycle.

Is there a difference between the fixed point and the limit cycle from the perspective of the power grid stability? The answer is yes, and it is related to the size of the stability basin of each one of the stationary solutions above as described in the next section.

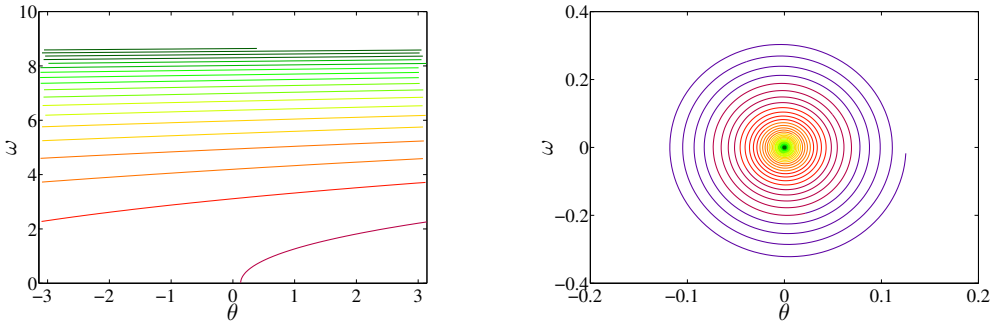

(a) (b)

Figure 3.2.: Trajectory of (θ, ω) starting at fixed point (as defined in equation 3.5). Beginning with time $t = t_0$ the trajectory is violet and at $t = t_{\text{end}}$ it is dark green. Then (a) K is set to zero. This could be the case if the transmission line suffers a short circuit and (b) P is set to zero. E.g. the turbine has to be shut down.

3.2. Stability basin

Returning to the breakdown of the transmission line. In the former case the generator returns to its intended fixed point (FP). This normally occurs when the starting values are close to the FP one therefore speaks of a *stability basin* around that attractor.

And in the latter case the generator finally has a fluctuating frequency whose mean is different from zero. That means it does not run synchronous with the grid.

Now we can divide the phase-space into two regions. The first in which started trajectories converge to the FP and another region where trajectories end in the limit cycle. The first region covers all ICs that guarantee synchronous regime of the single node. The second can be thought as bringing the power grid to failure. A section $(\theta, \omega) \in [-\pi, \pi] \times [-15, 15]$ of the phase space is shown in figure 3.3 where the orange (brighter) part contains all IC of trajectories that are attracted by the FP.

Having defined stability basin in phase-space, a good measure of stability for the single node would be given by the size of the stability basin [4] namely

$$\mathcal{S}_{\text{B}} = \int \chi\left(\theta, \omega\right) \rho\left(\theta, \omega\right) \, \mathrm{d}\theta \, \mathrm{d}\omega, \tag{3.8}$$

with χ equal to one, if (θ, ω) belongs to the basin (orange region in figure 3.3) and zero otherwise and the normalization $\int \rho\left(\theta, \omega\right) \, \mathrm{d}\theta \, \mathrm{d}\omega = 1$. Therefore the *basin stability measure* $\mathcal{S}_{\text{B}}$ is a number between one and zero. If $\mathcal{S}_{\text{B}} = 1$ every trajectory converges to the FP.

For the case illustrated in figure 3.3 with $P = 1$, $K = 8$ and $D = 0.1$ we obtain $\mathcal{S}_{\text{B}} \approx 0.39$. The approximation is because of the finite step size in starting values of the trajectories. In this example $\Delta\theta = 0.1$ and $\Delta\omega = 0.1$ has been used, yielding about 19000 measured points.

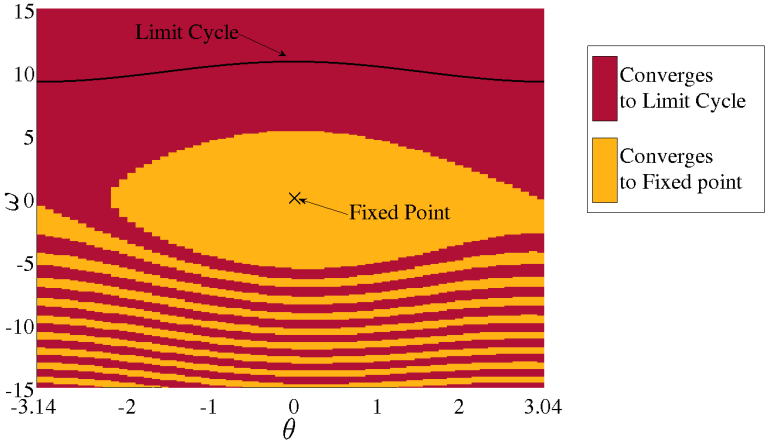

Figure 3.3.: A section from the (θ, ω)-space of the single node with $P = 1$, $K = 8$ and $D = 0.1$. The part in which the started trajectories reach the fix point is marked in orange the other part in which trajectories reach the limit cycle is marked red.

For values of $\omega \in [-100, 100]$ which will be used from now on (to be consistent with [4]), we have to calculate about 126000 trajectories. This is possible for one generator but in larger networks this costs a lot of time (about 120 hours for one node with $N_\mathrm{n} = 100$ on one CPU).

This problem encourages another method for calculating $\mathcal{S}_\mathrm{B}$. We take N_t uniformly distributed starting values of $(\theta, \omega) \in [-\pi, \pi] \times [-100, 100]$ and calculate the trajectory. If it ends in an ϵ-sphere around the FP, we add up a counter, say T. For N_t big enough the IC cover homogeneously most of the investigated phase space and the stability basin area is approximately

$$\mathcal{S}_\mathrm{B} = \frac{T}{N_\mathrm{t}} \ . \tag{3.9}$$

This raises the question how much trajectories are needed? In other words how does the error of this estimate decrease with N_t. In figure 3.4 the dependence of $\mathcal{S}_\mathrm{B}$ on N_t is shown.

Figure 3.4 displays that the error of $\mathcal{S}_\mathrm{B}$ decreases fast in the interval $N_\mathrm{t} \in [0, 500]$ but slow for higher N_t. To get a qualitatively statement one can use 500 trajectories. That implies an error of about ten percent for a single measurement and a standard deviation of $\sigma = 0.023$ [4]. It is better to use 1000 or more where the error of a single event is about five percent.

This method allows to investigate changes of $\mathcal{S}_\mathrm{B}$ when parameters are varied. For instance one may expect that the basin stability increases when K grows since the grid remains always in steady state and with larger K the coupling dominates the behaviour of the single node. In figure 3.5(a) $\mathcal{S}_\mathrm{B}$ is plotted against K.

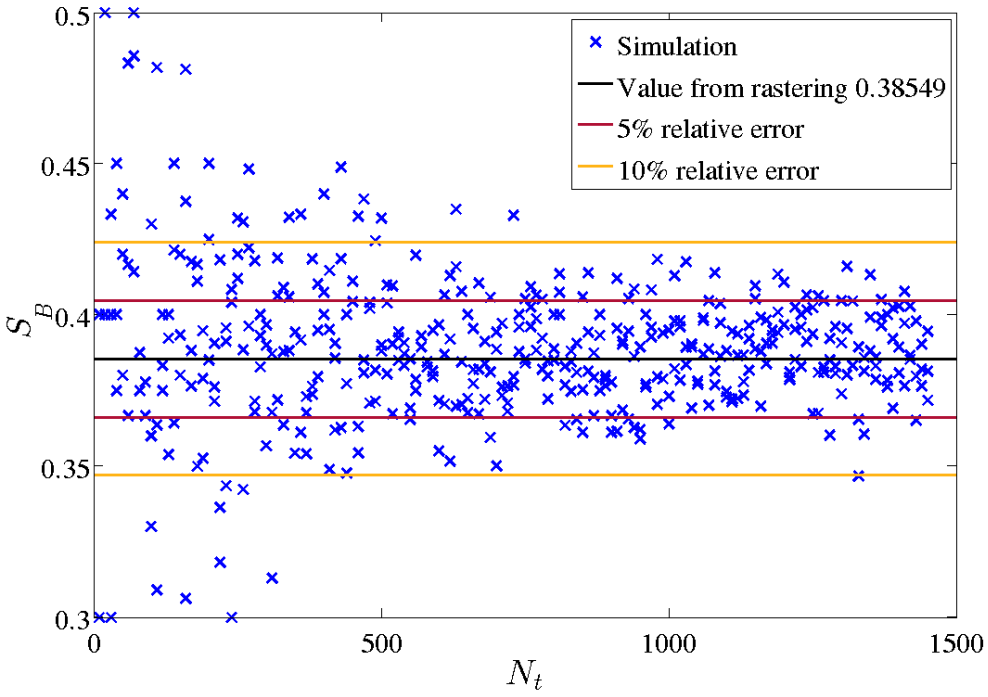

Figure 3.4.: Dependence of $\mathcal{S}_\mathrm{B}$ on N_t for $\epsilon = 0.1$ and the same parameters as in figure 3.3.

The figure 3.5(a) shows that the stability of the node indeed has a tendency to increase with larger coupling strength. It is also interesting to observe that at $K = 62$ there exists a transition from $\mathcal{S}_\mathrm{B} \approx 0.54$ to $\mathcal{S}_\mathrm{B} = 1$.

This result encourages the use of the region $(\theta, \omega) \in [-\pi, \pi] \times [-100, 100]$ in state space since it shows an interval with $\mathcal{S}_\mathrm{B} = 0$ another with $\mathcal{S}_\mathrm{B}$ monotonically increasing and a third where $\mathcal{S}_\mathrm{B} = 1$ [4].

Next we briefly consider the damping D in equation 3.1. Since D weights the relaxation towards the FP, one can intuitively understand that the damping also increases the basin stability as shown in figure 3.5(b). The fact that the damping is primarily a result of the automatically primary control mechanisms of the power grids [10] implicates that there is usually little scope to the damping ratio. Therefore the idea of dramatically increasing D to raise basin stability is negligible.

We will return to this stability measure in the context of the multi-node model in chapter 4. In the case of multiple nodes not only the parameters of every node is important but rather the connection between the nodes or more specifically the topology plays a fundamental role in the grid stability.

In this chapter we will continue with a more detailed description of the perturbation of the single node, when subjected to the power fluctuation.

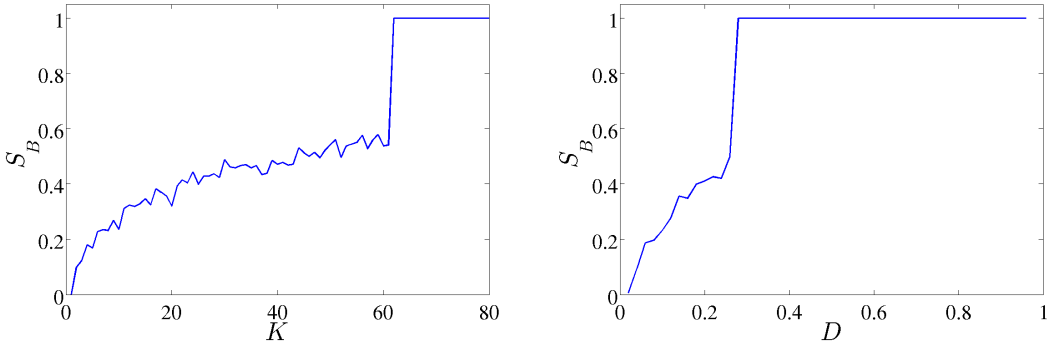

(a) (b)

Figure 3.5.: Basin statbility $\mathcal{S}_\mathrm{B}$ for different K values with $P = 1$, $D = 0.1$, $N_\mathrm{t} = 500$ and $(\theta, \omega) \in [-\pi, \pi] \times [-100, 100]$.

3.3. Fluctuating power input

With the increasing number of renewable energy sources like wind turbines and solar panels a new challenge for the power grid design arises besides ensuring the power supply namely the power fluctuations on small times scales.

For wind turbines magnitudes down to seconds are relevant [13]. Furthermore the translation from wind velocity to power is a stochastic process itself. The development of an universally valid model to describe the wind power with all its features is a difficult task and recently discussed by [14]. But it is known that the distribution of increments of the wind velocity and also power production show a non gaussian behaviour with a fourth momentum.

In this chapter we will focus on a single generator whose power input follows a stochastic process that has crucial properties in common with the fluctuation of wind power. Since we mainly want to study the differences between a *gaussian* and *non gaussian* statistic (the precise meaning is described later) a simple model is used with that we are able to change the non gaussian features in a controlled way.

The equation of the single node model for the angular velocity becomes

$$\dot{\omega} = -D\omega + P(t) - K \sin(\theta) \tag{3.10}$$

where the power as a function of time reads

$$P(t + \Delta t) = P(t) - D_1 \Delta t + D_2 \sqrt{\Delta t} \eta(t) \tag{3.11a}$$

$$D_1 = (P - P_0) \tag{3.11b}$$

$$\log(D_2(t + \Delta t)) = \log(D_2(t)) - (\log(D_2(t)) - a)\Delta t + |b|\sqrt{\Delta t}\eta'(t) \tag{3.11c}$$

The equations (3.11a) to (3.11c) contain a lot of new parameters that need some explanation. At first we assume $b = 0$ what is equivalent to D_2 is a constant. Then

$P(t)$ is a stochastic variable that fluctuates in time with a mean $\mu = P_0$ and a standard deviation of $\sigma = D_2$. An example process is shown in figure 3.6. Thereby $\eta(t)$ is a normal distributed random variable with mean zero and standard deviation two which is responsible for the randomness in the process. The coefficient D_2 weights the fraction of the fluctuation while D_1 controls the relaxation to the mean value P_0. This case is called *gaussian* process or power fluctuation.

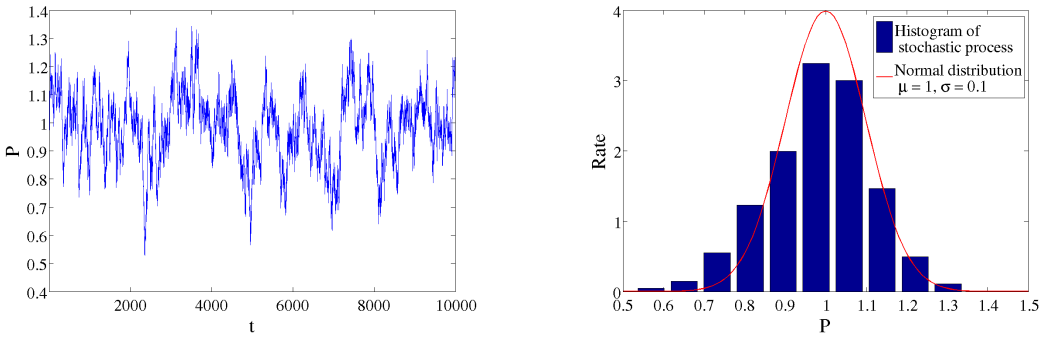

(a) (b)

Figure 3.6.: (a) Realization of the stochastic process defined by equation (3.11a) and (3.11b) with $P_0 = 1$ and $D_2 = 0.1$. (b) Histogram of the stochastic variable P that follows the stochastic process shown in the figure to the left compared to a normal distribution with mean 1 and standard deviation 0.1.

If b is now increased the standard deviation is no constant any more but rather a random variable itself. This results in an fourth momentum or more precisely a kurtosis γ in the power distribution which can be calculated by

$$\gamma = e^{4b^2} + 2e^{3b^2} + 3e^{2b^2} - 6 \tag{3.12}$$

and we therefore call that case *non gaussian* power fluctuation. If we furthermore choose $a = \log(\sigma) - b^2/2$ the mean standard deviation of the process for the power equals that of the constant $D_2 = \sigma$. On this view we can compare the gaussian power fluctuation with the non gaussian for a given standard deviation. As a last note η' is the same distribution as η. The apostrophe marks that there are two different random numbers are drawn independently from each other.

We now return to the single generator and convert it to a wind turbine by including the stochastic process as in equation (3.10). It is assumed that the generator works at the fixed point at $t = t_0$.

Then we calculate the trajectory of (θ, ω) and observe weather it becomes attracted by the limit cycle. To get a feeling how often this happens, we let the process run for some time, say one million iterations and do a two dimensional histogram in (θ, ω). Two examples are shown in figure 3.7.

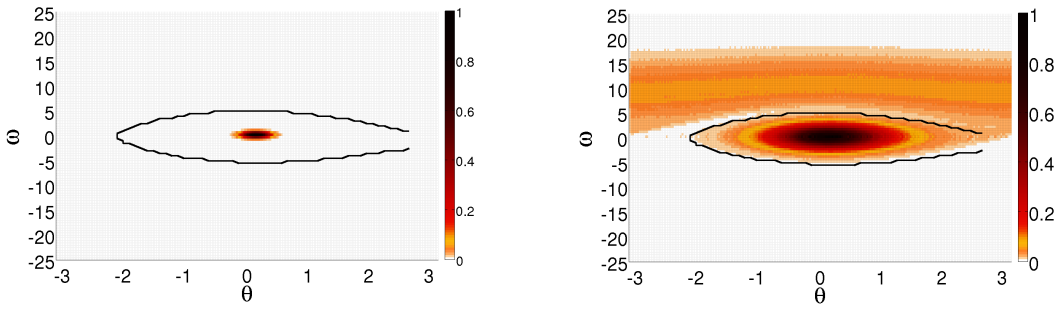

(a) $\sigma = 0.5$ and $b = 0$.

(b) $\sigma = 1.0$ and $b = 0$.

Figure 3.7.: Histogram of how often the trajectory passes a little cube in (θ, ω) phase space for different standard deviations. The black line marks the stability basin of the single node without fluctuating power.

For a standard deviation of 0.5 the trajectory moves around the fixed point, as shown in figure 3.7(a). Its *density* is peaked at that point, meaning the frequency of appearance in a single cube in phase space which becomes a density in the cube size to zero limit.

If the standard deviation increases the width of the trajectory density also grows. When the density at the borders of the stability basin rises above zero, the trajectory is able to escape the fixed point stability basin of the single node without fluctuation (also called *deterministic process* in the following) and runs to the limit cycle. Since the fluctuation of the power is big enough to escape the limit cycle, too, it can return to the fixed point of the deterministic process.

For the standard deviation of 1.0 as shown in figure 3.7(b) the density around the fixed point is still much larger than that of around the limit cycle but the latter is already not negligible. Hence this situation would be rated as unstable or not synchronous and should be avoided.

At this point the question arises if the process with non gaussian power fluctuation shows a significant different behaviour. When the kurtosis of the fluctuation becomes larger one may expect that there are more possibilities for the trajectory to escape the fixed point and hence the density around the limit cycle will also increase. This is indeed the case as illustrated in figure 3.8.

Another interesting observation is that the density at the boundary of the stability basin of the deterministic process is zero. Therefore the trajectory does not need to reach this boundary often to escape the stability basin. Instead it can move out suddenly and unexpected what makes the situation even more dangerous in the view of stability or synchronization.

So what is the critical b for a given σ? This dependence can be done more systematically when we consider that the deviation of the trajectory from the fixed point is symmetric in the stable situation and asymmetric when the density around the limit cycle rises. Therefore we investigate the covariance of θ and ω. It is plotted in figure 3.9.

From figure 3.9 we can learn that for given σ the b and hence the kurtosis γ decrease

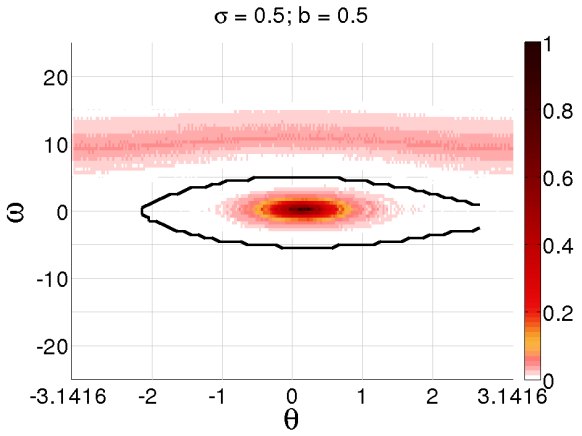

Figure 3.8.: Histogram of the trajectory in (θ, ω) phase space for $\sigma = 0.5$ and $b = 0.5$. The black line marks the stability basin of the single node without fluctuating power.

the probability for the trajectory to stay at the fixed point as the absolute value increases from zero. Furthermore we notice that the covariance converges to zero again for large σ and b. For these high values the fluctuation of the trajectory becomes so large that it does not feel any attraction from the fixed point or the limit cycle and therefore cover the whole investigated state space homogeneously. In that case the covariance becomes zero again. The conclusion is that the variance of θ or ω should always be investigated together with the covariance.

To conclude this chapter we note that the power fluctuation is an alternative way to model perturbations in a power grid or more precisely in a single node so far. Such an investigation for multiple nodes is not done in this work but will be examined in future publications. The model for the fluctuations is a very simplified one but contents an important property of the stochastic wind power namely the kurtosis and therefore rare events in the increments of the power.

Since it is just a probability if the trajectory is in the limit cycle or near the fixed point the basin stability is no valid measure for this kind of perturbation. For qualitatively statements the covariance combined with the variance of the phase angle or angular velocity is a convenient variable.

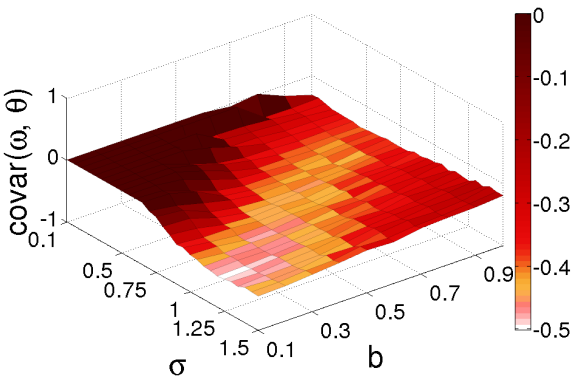

Figure 3.9.: Covariance of θ and ω in dependence on σ and b.

4. Multi node model

Power grids, as the name already suggests, consist of a set of nodes (which are the generators and loads) and a set of connections (which are the transmission lines) between them. The generators and consumers interact with each other and can be described as coupled oscillators via the swing equation introduced in section 2.7.

A grid consisting of multiple nodes with homogeneous coupling constants $K_{ij} = K = 8$ has been investigated by Menck et al. [4] considering nodes as effective consumers or generators with power $P = -1$ or $P = +1$ respectively.

In this chapter we will follow this concept and study random generated networks with the basin stability approach known from Section 3.2 which shall be understood in a slightly different way: All nodes run at their prescribed frequency and angle or in other words the grid is in the steady state. Thereafter one node is deflected to some point in state space (θ, ω). The convergence criteria now is that the trajectories of *all* nodes must run back into an ϵ-sphere around their specific fixed point $(\theta_{\mathrm{SS},i}, 0)$.

This chapter has two parts. First it provides in Section 4.1 with an overview of random network generation and different types of networks. Then in Section 4.2 the equations modified to the multi node model are presented as well as the results of the stability distribution. A grid with heterogeneous coupling strengths, power production and consumption together with some other important parameters for describing actual power grids will be analysed in the last Chapter 5 of this thesis.

4.1. Generation of random networks

To investigate a network with multiple nodes we need not only the parameters of every generator but rather the topology or more precisely the adjacency matrix $\mathcal{A}$. There are two possibilities to obtain it. We can use a topology of a grid that exist in reality or create it in a certain way.

Since it is accompanied by a lot of effort to collect and process realistic power grid data, we will first take a look at the random generation of networks. An important requirement on the random graph generation algorithm is that it reproduces the essential properties of the real power grids. These are basically the clustering coefficient and the average shortest path length introduced in Section 2.2. Typically power grids have a relatively small clustering coefficient and average shortest path length, see Table 4.1.

There are several algorithms for every category of networks. Here two of them are mentioned exemplarily for a crucial network structure respectively namely random network and small world network.

The Erdös-Rényi (ER) algorithm was introduced in 1959 by Erdös and Rényi [16]. The algorithm operates as follows.

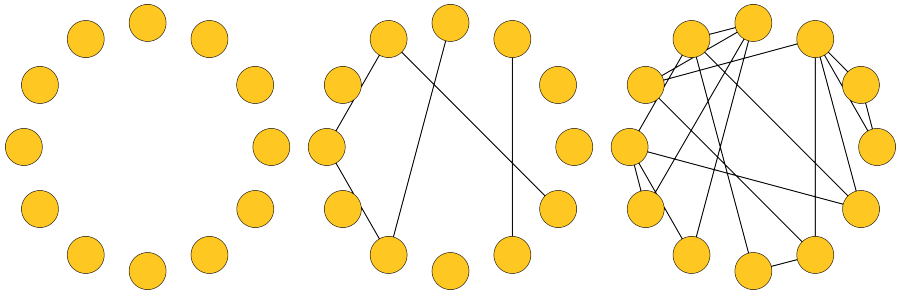

Figure 4.1.: Illustration of the Erdös-Rényi algorithm. The nodes are initialized then a connection is added in every step with probability p.

We choose a desired number of nodes N_n and store their properties in an ordered way. After the initialization we visit every pair i, j of nodes and connect them with a given probability p and continue until the desired number N_edge of connections is reached. A *connection* process between node i and j is defined by setting $(\mathcal{A})_{ij} = 1$. If the network is weighted $(K)_{ij} = k_{ij}$ and if is undirected we set $\mathcal{A}_{ji} = \mathcal{A}_{ij}$ and $K_{ji} = K_{ij}$.

The algorithm is illustrated in Figure 4.1.

The resulting graph is usually called a *random graph* as introduced in Section 2.2. Since power grids match best with random networks this algorithm is suitable for the generation.

Another indispensable feature of power grids is that the are no nodes or clusters that are not connected to all other nodes. In other words it must be possible to reach every node from any other through an arbitrary number of connections. We will call this property *unsplit* from now on. A network created by the ER algorithm is typically unsplit if $p > p_c \approx 1/N_\mathrm{n}$. It is not trivial to implement the algorithm in a way that it generates only unsplit networks if we do not want to reject created networks which are split. It is easier with another algorithm, the Watts-Strogaz-algorithm [15].

We initialize the nodes as composing a regular network by connecting each node i with its k next neighbours, as shown in figure 4.2(a). In the next step we visit every connection and reconnect it with probability p. When the reconnection takes place the connection i to j will be changed into i to j' where it can be any node except for i. Furthermore the network must not contain double connection. Note however that it is also possible with probability $1/N_\mathrm{n}$ that $j' = j$.

	average shortest path length	clustering coefficient (max = 1)
Film actors	3.65	0.79
Power grids	18.7	0.080
Neurons	2.65	0.28

Table 4.1.: Summeration of typical values of different network structures [15].

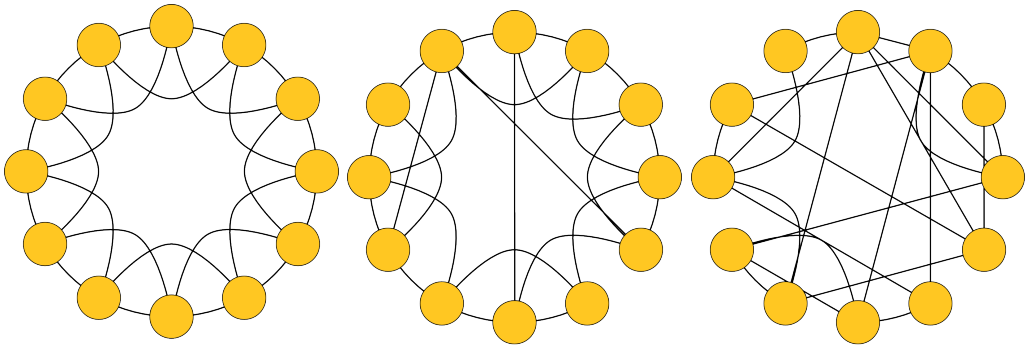

regular
(a) Initialization or $p = 0$

small world
(b) $p \approx 0.001$

random
(c) $p = 1$

Figure 4.2.: Network generated by the Watts-Strogaz algorithm with different probabilities p for reconnecting connections.

With larger probability p also the number of reconnection increases and the grid becomes less regular. Therefore the clustering coefficient decreases and the graph turns more and more into a random graph as illustrated in figure 4.2(c).

It is interesting to notice that the average shortest path length dramatically decreases for p slightly above zero due to the resulting shortcuts connecting clusters that remain from the regular structure [15]. Consequently we are able to tune the network with p from regular over small world to random network. In this work we will use the Watts-Strogaz algorithm with $p = 1$ to create a random network.

For complex networks containing thousands or more nodes with an average node-degree $\langle d \rangle \gg \log(N_\mathrm{n})$ it is guaranteed that the reconnection process leads to an unsplit network. Since the condition $\langle d \rangle \gg \log(N_\mathrm{n})$ does not hold for power grids with $N_\mathrm{n} \approx 100$, we need to check after every reconnection if the grid is split. If this is the case, the reconnection has to be undone.

4.2. Stability distribution in networks of multiple nodes

The grid consists of N_n nodes where the frequency of every node follows an equation like (3.1).

Since the damping results only from the automatically primary control which is the same for every component of the grid, we set all $D_i = D = 0.1$ following the idea of [4] in order to focus on the topology, the power is set depending on node i being generator ($P_i = +1$) or consumer ($P_i = -1$). The interaction of the nodes of cause affects the coupling term. The nodes couple to each other due to their phase angle as described in Section 2.7. As a first approximation we equalize all coupling constants $K_{ij} = K_{ji} = 8$ [4], if node i and j are connected and zero otherwise.

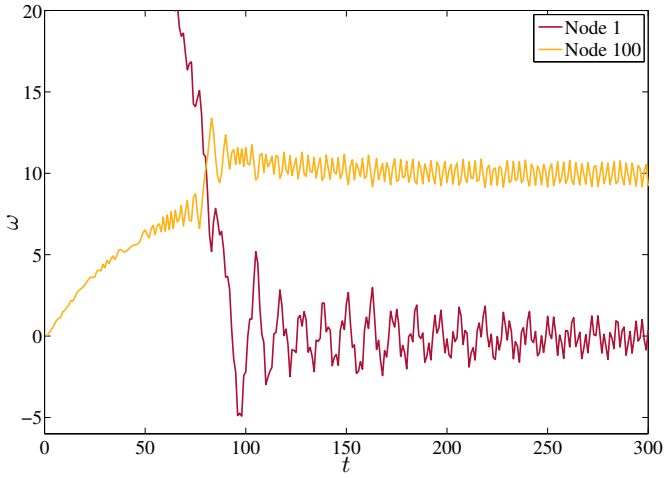

Figure 4.3.: Frequency of two nodes over time. Node 1 is perturbed and returns to the initial state, while node 100 gets perturbed due to the coupling with node one and its frequency converges to the limit cycle.

These assumptions lead to

$$\dot{\omega}_i = -D\omega_i + P_i - \sum_j^{N_\mathrm{n}} K_{ij} \sin\left(\theta_i - \theta_j\right), \tag{4.1}$$

$$\dot{\theta}_i = \omega_i, \tag{4.2}$$

with $D = 0.1$, $P = \pm 1$ and $K_{ij} = 8\mathcal{A}_{ij}$. The adjacency matrix $\mathcal{A}_{ij}$ is obtained by random generation through a Watts-Strogaz-algorithm as described in previous Section 4.1.

To characterize the stability of every node, we apply the basin stability in a modified way. As described for a single node in Section 3.2, the basin stability is the fraction of initial conditions (IC) in state space (θ_i, ω_i) for trajectories that reach the fixed point (FP) given by

$$(\theta_i, \omega_i) = (\theta_{\mathrm{SS},i}, 0) \ . \tag{4.3}$$

The basin stability (BS) is a measure only for the perturbation of one node so the IC for all other nodes are $(\theta_j, \omega_j) = (\theta_{\mathrm{SS},j}, 0)$. Therefore the BS does not give any information about which node is or is not in FP after perturbation of node i. It may for instance be the case that node i returns to its steady state but its neighbour j runs at a limit cycle because the coupling with the node i propagated the perturbation to node j, see figure 4.3.

As an example, we now generate a net with $N_\mathrm{n} = 100$ and $N_\mathrm{edge} = 135$ connections. A part of it is illustrated in Figure 4.4(a). The BS for this net is plotted for every node

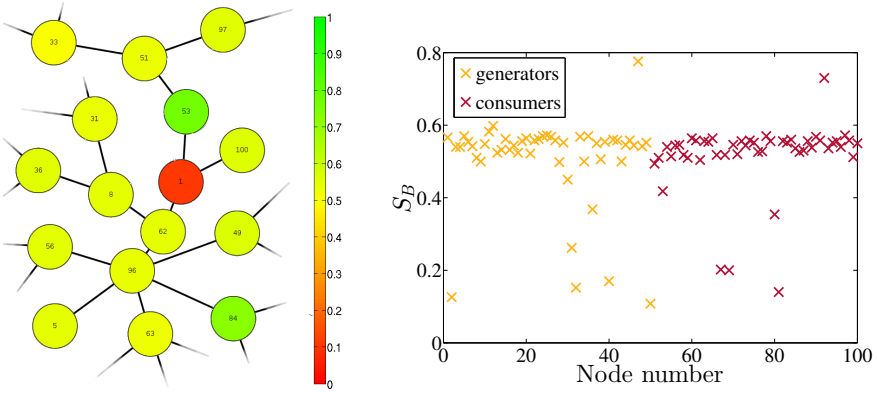

(a) (b)

Figure 4.4.: (a) Part of the example random generated network with 100 nodes discussed in the text. The color of the nodes corresponds to their basin stability $\mathcal{S}_\mathrm{B} \in [0, 1]$. (b) The Basin stability $\mathcal{S}_\mathrm{B}$ for every node respectively. The nodes are sorted depending on being generators or consumers.

in Figure 4.4(b) where the numbers of the nodes are rearranged in the way that 1 to 50 are the generators and 51 to 100 are the consumers.

Does this example represent the typical case for power grids? To answer this question we generate an ensemble of 100 grids. Figure 4.5(b) shows the histogram of BSs of all 10000 nodes in this ensemble and Figure 4.5(a) of the first 100 nodes. The comparison points out that this is indeed the case for $\mathcal{S}_\mathrm{B} < 1$ while there is another noticeable feature of the histogram that is clearer in Figure 4.5(b) namely a three-peak-structure.

There are two broad peaks with maxima at $\mathcal{S}_\mathrm{B} \approx 0.2$ and $\mathcal{S}_\mathrm{B} \approx 0.5$ and one sharp peak at $\mathcal{S}_\mathrm{B} \approx 1$. Since the parameters of all nodes are the same, the reason of these significant differences in the stability of the nodes must be the topology of the grid.

As observed in the single node model (Chapter 3) the coupling constant K changes the stability of a node. We can therefore imagine that the number of coupled nodes has a similar effect. A useful way to investigate this behaviour is a correlation between the number of neighbours (or even the neighbours of the next-neighbours) and the BS. To analyse this we look at the average degree d_av as a new quantity that can be calculated as

$$d_{\mathrm{av},i} = \frac{1}{d_i} \sum_{j,K_{ij}>0}^{N_\mathrm{n}} d_j \tag{4.4}$$

The dependence of the node-degree and its neighbours average node-degree is illustrated in Figure 4.6.

Nodes with degree one have a BS of about one half independent of the average degree of their neighbours. These nodes are called *dead ends*. If a perturbation occurs in such

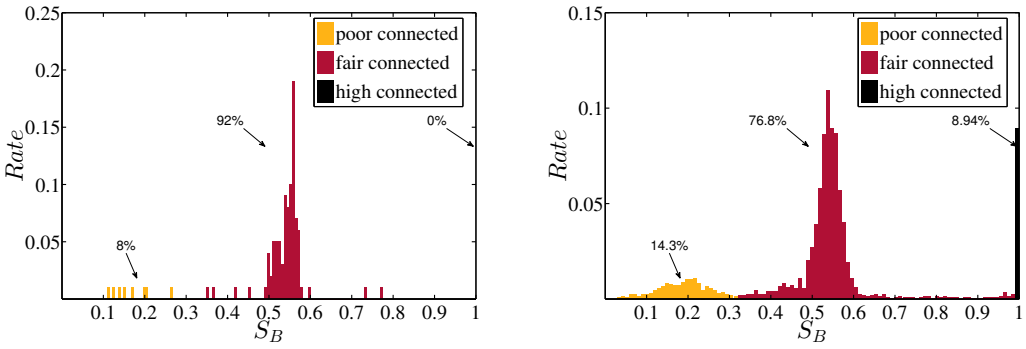

(a) (b)

Figure 4.5.: Comparison of the distribution of BS in (a) a random power grid and in (b) an ensemble of 100 grids.

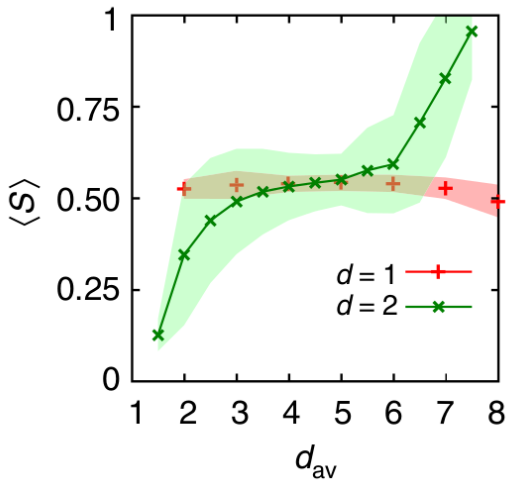

Figure 4.6.: Dependence of BS from the number of a nodes neighbours and the average degree of their neighbours. Figure from [4].

a dead end, the case is similar to the single node case. The unperturbed connected node has a damping influence on the fluctuation but in this case the phase angle of the connected nodes gets elongated, too. In a dead end the effective coupling to the grid is smaller than for the idealistic single node.

This situation changes if the perturbed node is connected to two other nodes of the grid. The fluctuation can then propagate further into the grid and the effective coupling becomes larger. If one of the neighbours is a well connected node of $d_{\mathrm{av},i} \gtrsim 8$ the BS increases to one. Therefore the sharp peak in figure 4.5(b) can be explained by nodes having a high average degree [4]. On the other hand the peak at $\mathcal{S}_{\mathrm{B}} \approx 0.2$ can be explained by nodes being near dead end, meaning they have a neighbour with average node degree two or less.

From this chapter we can conclude that dead ends should be avoided in grids with homogeneous coupling constants and power. In the next chapter we investigate whether this also holds for power grids with heterogeneous properties which are therefore more realistic.

5. Realistic power grids

In the previous chapters power grids have been investigated with a model containing advanced variables that have been chosen randomly or by assumptions [4]. In this section we will look at an existing grid whose whole properties are available in public [11].

To understand how it is possible to obtain a model similar to that one used before, we will first discuss an extended transmission line model. Then we address the so called *Kron-Reduction* since models based on a given admittance matrix mostly contain this reduction. Afterwards an overview of three models that have already been studied in the literature is given [2].

When all components needed for description of the more realistic power grids are addressed we will exemplarily calculate the stability of the "IEEE-50gen"-network.

5.1. Extended transmission line model

To obtain a coupling matrix K from real transmission line data for the further calculation, it is necessary to use a complex model for the transmission lines. The branches consist of a π-model with series impedance $Z_s = R_s + iX_s$ and parallel (total) line charging susceptance B_c in series with an ideal phase shifting transformer, as shown in figure 5.1. As a consequence of this model a transmission line with a phase shifting transformer is not symmetric and the nodes at the ends are not identical. One speaks of a *from*-end and a *to*-end with I_f, V_f and I_t, V_t respectively. They are also called *tap*-end and Z-end regarding to the element near to the connection with the node, that is either the tap-/phase shift transformer or the impedance Z.

With an admittance $Y_s = 1/Z_s$ the following relation can be derived from Kirchhoff's and Ohm's law

$$\begin{pmatrix} I_\mathrm{f} \\ I_\mathrm{t} \end{pmatrix} = \begin{pmatrix} \left(Y_s + i\frac{1}{2}B_c\right)\frac{1}{\tau^2} & -Y_s\left[\tau\exp\left(-i\zeta\right)\right]^{-1} \\ -Y_s\left[\tau\exp\left(i\zeta\right)\right]^{-1} & Y_s + i\frac{1}{2}B_c \end{pmatrix} \begin{pmatrix} V_\mathrm{f} \\ V_\mathrm{t} \end{pmatrix} \tag{5.1}$$

We denote the elements of this branch-admittance matrix of jth branch from equation (5.1) by

$$Y^j_\mathrm{branch} = \begin{pmatrix} Y^j_\mathrm{ff} & Y^j_\mathrm{ft} \\ Y^j_\mathrm{tf} & Y^j_\mathrm{tt} \end{pmatrix} \tag{5.2}$$

where j is an index not an exponent here and in the following.

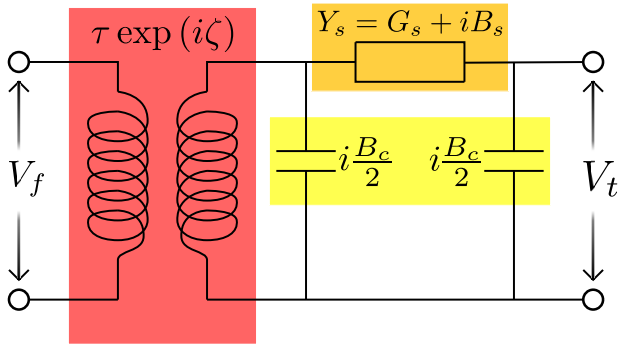

Figure 5.1.: Layout of a transmission line. A phase shifting transformer (red/dark box) connected in a series with an impedance Z_s (or admittance Y, orange box) and parallel to two capacitors (yellow/light box) which represent the total line charging susceptance B_c.

To get the admittance matrix Y_0 of the whole grid, all currents flowing from and to a node must be added up and Ohm's law has to be used again. This yields a current I_j for a node j

$$I^j = \sum_k I_{\mathrm{f}}^k + \sum_l I_{\mathrm{t}}^l = \sum_k \left(Y_{\mathrm{ff}}^k V^j + Y_{\mathrm{ft}}^k V^m \right) + \sum_l \left(Y_{\mathrm{tt}}^l V^j + Y_{\mathrm{tf}}^l V^m \right) \tag{5.3}$$

with all transmission lines k running from node j to node m and l running from m to j respectively and V the voltages of the nodes. Notice that a line running from j to m does not necessarily imply that current is injected from node j to that line. By rearranging of the Ys and Vs this leads to

$$\vec{I} = Y_0 \vec{V} \tag{5.4}$$

This procedure can be translated into linear matrix transformations as described in the following. See also chapter A.2 for an example.

We need the connection matrices C_{f} and C_{t} besides the admittance matrix for each branch. The $N_{\mathrm{l}} \times N_{\mathrm{n}}$ connection matrices with the number of nodes N_{n} and lines N_{l} are defined by

$$C_{\mathrm{f}}^{i,j} = \begin{cases} 1 & \text{if branch } i \text{ starts } \textit{from} \text{ node } j. \\ 0 & \text{otherwise} \end{cases} \tag{5.5}$$

And C_{t} analogously if branch i runs *to* node j. Then we obtain from-admittance-matrix Y_{f} and to-admittance-matrix Y_{t} by

$$Y_{\mathrm{f}}^{i,j} = C_{\mathrm{f}}^{i,j} Y_{\mathrm{ff}}^i + C_{\mathrm{t}}^{i,j} Y_{\mathrm{ft}}^i \tag{5.6}$$

$$Y_{\mathrm{t}}^{i,j} = C_{\mathrm{f}}^{i,j} Y_{\mathrm{tf}}^i + C_{\mathrm{t}}^{i,j} Y_{\mathrm{tt}}^i \tag{5.7}$$

In other words every row of $C_{\mathrm{f/t}}$ is multiplied by the admittance of the corresponding line, see example A.2.

Finally Y_0 can be calculated from

$$Y_0 = (C_{\mathrm{f}})^{\intercal}\, Y_{\mathrm{f}} + (C_{\mathrm{t}})^{\intercal}\, Y_{\mathrm{t}} + Y_{\mathrm{shunt}} \tag{5.8}$$

where Y_{shunt} is a diagonal matrix with the shunt losses to the ground. The coupling matrix K derived from Y_0 is dependent from the modelling of the consumers. A summary of existing models is given in Section 5.3.

5.2. Kron-reduction

The Kron-reduction is an algebraic operation that maps node relations of the set s of the N_{n} nodes of the network on a subset $s_\alpha = 1, ..., N_\alpha$ while conserving the interaction of the whole network. Mathematically this procedure is known in a more general context as the Schur complementation [17].

Lets consider the current-balance equation $I = YV$ derived from Ohms and Kirchhoffs law. To highlight the relation between the subsets s_α and $s_\beta = s \backslash s_\alpha$ of the nodes we can rearrange it to

$$\left(\frac{I_\alpha}{I_\beta}\right) = \left(\begin{array}{c|c} Y_{\alpha\alpha} & Y_{\alpha\beta} \\ \hline Y_{\beta\alpha} & Y_{\beta\beta} \end{array}\right) \left(\frac{V_\alpha}{V_\beta}\right) \ . \tag{5.9}$$

A Gauss-elemination of the part $Y_{\alpha\beta}$ yields [17]

$$I_\alpha - Y_{\alpha\beta} Y_{\beta\beta}^{-1} I_\beta = Y^{\mathrm{red}} V_\alpha \ . \tag{5.10}$$

Nodes with current zero are called *passive* nodes, in other words their current-injection equals the current-ejection. If the subset s_β contains only passive nodes I_β is zero and we obtain a relation between the currents and voltages of subset s_α

$$I_\alpha = Y^{\mathrm{red}} V_\alpha \ . \tag{5.11}$$

In this case the Kron-reduction can be expressed more algorithmically by

$$Y_{ij}^{\mathrm{red}} = Y_{ij} - \frac{Y_{ik} Y_{kj}}{Y_{kk}}, \tag{5.12}$$

where k is the node that should be reduced.

A simple example is the Y-Δ transformation shown in Figure 5.2. The mathematical execution of the reduction process is demonstrated in Section A.1.

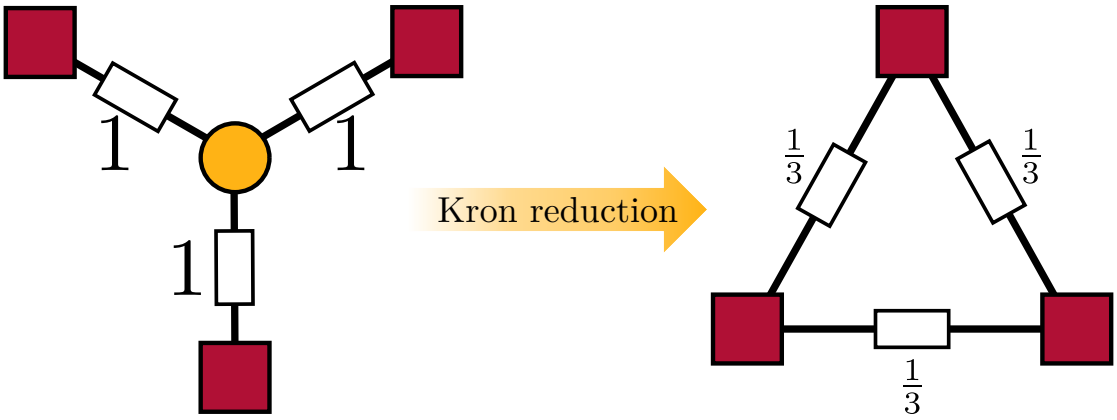

Figure 5.2.: Illustration of the Y-Δ transformation. A network shaped as a Y contains a passive node represented by the orange circle in the middle that will be reduced. The remaining network is shaped as a Δ.

5.3. Effective Network, Synchronous Motors and Structure Preserving model

Power grids are large non-linear systems. Thus the problem of describing the influence of the large scale network to the dynamics of the components is, despite the extensive literature, not completely answered in detail. With the increasing number of researchers working on the topic different models arose.

These can basically be divided in three groups. All of them are using a network of coupled oscillators, whose dynamic is governed by

$$\frac{2H_i}{\omega_\mathrm{r}}\frac{\mathrm{d}^2\theta_i}{\mathrm{d}t^2} = -D\frac{\mathrm{d}\theta_i}{\mathrm{d}t} + A_i - \sum_{j=1,j\neq i}^{N_\mathrm{n}} K_{ij}\cos\left(\theta_i - \theta_j + \phi_{ij}\right), \tag{5.13}$$

as fundamental part. The main task of every model is defining A^{model} and K^{model}. While the generators are uniformly modelled by Equation (5.13), there exist several models for the loads.

In the first group they are described as constant impedances connected to the ground, whereby the energy consumption of the loads is regarded as losses over that impedance. This so-called *effective network* (EN) model results in an effective interaction between the generators and does not conserve the physical structure of the grid since the loads are passive elements that can be reduced.

The loss of the physical structure can be prevented when describing also the loads as oscillators. This is done by the so-called *structure preserving* (SP) model by applying a first order swing equation for the loads, obtained by setting their inertia to zero. Therefore the equations for generators and loads (including terminal nodes explained in the following) are different. Furthermore the equation system becomes larger due to the terminal nodes.

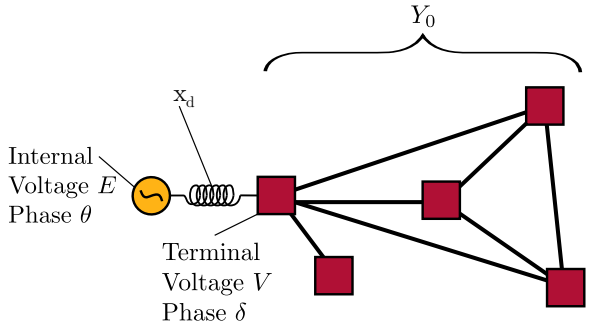

Figure 5.3.: The physical network Y_0 is extended by internal nodes (here only one is shown in orange) which are connected to the terminal nodes, coloured in red, by a transient reactance x_d.

A third model applies the whole swing equation for the loads leading to a network of synchronous machines emphasizing the name *synchronous machines* (SM) model. It does not preserve the structure of the network during the calculation process but all information needed to reconstruct it at any desired step.

An important concept, that has been already mentioned, is the separation of nodes into internal and terminal nodes. The latter can be regarded as a transformer station which connects the power plant or the consumer with the transmission grid that we derived as Y_0 in Section 5.1. The internal node represents the rotating mass itself. They are connected by a so-called transient reactance x_d as shown in Figure 5.3. The terminal node has itself a voltage $V = |V| \exp(i\delta)$ while we call the voltage of the internal node $E = |E| \exp(i\theta)$. By expressing the current I in $P + iQ = VI^*$ through Ohm's law $ix_\mathrm{d}I = E - V$ the magnitude of E is obtained

$$|E|^2 = \left(\frac{Px_\mathrm{d}}{|V|}\right)^2 + \left(|V| + \frac{Qx_\mathrm{d}}{|V|}\right)^2 \ . \tag{5.14}$$

Additionally the real part yields the power angle equation

$$P = \frac{|EV|}{x_\mathrm{d}} \sin(\theta - \delta) \ . \tag{5.15}$$

In the following the models are addressed in more detail.

Effective network model (EN)

The loads are described as constant admittances $Y_{l,j} = (P_{l,j} - iQ_{l,j}) / |V_j|^2$ with the (active) demand P_l and have hence no dynamic. The synchronization process is shifted to the generators only and the loads affect them indirectly. Thus the dynamic of the system is investigated on time scales allowing the assumption of constant demand while being long enough to observe the phenomenon of synchronization.

The influence of the loads on the generators is included in the coupling matrix K having not the same entries occupied as the Y_0 matrix. In other words the topology changes during the transformation of Y_0 to K that operates as follows.

We re-index the nodes in such a way, that indices $j = 1, ..., N_g$ are generators and $j = N_g + 1, ..., N_\mathrm{n}$ are the loads, where N_g is the number of generators. The admittance matrix as derived in Section 5.1 hence has the form

$$\mathbf{Y}_0 = \begin{pmatrix} \mathbf{Y}_0^{gg} & \mathbf{Y}_0^{gl} \\ \mathbf{Y}_0^{lg} & \mathbf{Y}_0^{ll} \end{pmatrix}, \tag{5.16}$$

with the indices g and l meaning the coupling of a generator or load with another one of these two respectively. The connections between the internal and terminal nodes can be described by an admittance matrix $\mathbf{Y}_\mathrm{d}$ which, considering $I_g = (ix_\mathrm{d})^{-1}(E - V_g)$, has the transient reactances on its diagonal $Y_{\mathrm{d},jj} = (ix_{\mathrm{d},j})^{-1}$. With $\tilde{Y}_0 = Y_0 + \mathbf{E}\vec{Y_l}$ complete matrix reads

$$\mathbf{Y}_0' = \left(\begin{array}{c|c|c} \mathbf{Y}_\mathrm{d} & -\mathbf{Y}_\mathrm{d} & \mathbf{0} \\ \hline -\mathbf{Y}_\mathrm{d} & \tilde{\mathbf{Y}}_0^{gg} + \mathbf{Y}_\mathrm{d} & \mathbf{Y}_0^{gl} \\ \hline \mathbf{0} & \mathbf{Y}_0^{lg} & \tilde{\mathbf{Y}}_0^{ll} \end{array}\right) . \tag{5.17}$$

Since the terminal nodes and loads are passive ($I_i = \sum_j I_{ij} = 0$) the block $-\mathbf{Y}_\mathrm{d}$ in the first row of $\mathbf{Y}_0'$ can be reduced by Kron-reduction emphasizing the name effective or reduced network model. The remaining matrix is [2], [17]

$$\mathbf{Y}^\mathrm{EN} = \mathbf{Y}\left(\mathbf{1} + \mathbf{Y}_\mathrm{d}^{-1}\mathbf{Y}\right)^{-1}, \tag{5.18}$$

with

$$\mathbf{Y}' = \tilde{\mathbf{Y}}_0^{gg} - \mathbf{Y}_0^{gl}\left(\tilde{\mathbf{Y}}_0^{ll}\right)^{-1}\mathbf{Y}_0^{lg}, \tag{5.19}$$

and $\mathbf{1}$ a $N_g \times N_g$ identity matrix.

Concluding the model the full equation of motion is Equation (5.13) with [2]

$$A_i^\mathrm{EN} = P_i - |E|^2 G_{ii}^\mathrm{EN} \quad \text{and} \quad K_{ij}^\mathrm{EN} = |E_i E_j Y_{ij}^\mathrm{EN}| \ .$$

Structure preserving model (SP)

Another approach is to model the loads and also the terminal nodes as first order oscillators. This is motivated by assuming the inertia of these components as well as the deviation of the phase angle are small enough such that $H\ddot{\theta} \approx 0$. Since all nodes of the network have an inherent dynamic no reduction takes place and $\mathbf{Y}_0' = \mathbf{Y}^\mathrm{SP}$ that is given by [2]

$$\mathbf{Y}^\mathrm{SP} = \left(\begin{array}{c|c|c} \mathbf{Y}_\mathrm{d} & -\mathbf{Y}_\mathrm{d} & \mathbf{0} \\ \hline -\mathbf{Y}_\mathrm{d} & \mathbf{Y}_0^{gg} + \mathbf{Y}_\mathrm{d} & \mathbf{Y}_0^{gl} \\ \hline \mathbf{0} & \mathbf{Y}_0^{lg} & \mathbf{Y}_0^{ll} \end{array}\right) . \tag{5.20}$$

The only connection of every generator i is to its terminal $i + N_g$ (after re-indexing as in EN model) node and their coupling is described by Equation (5.15). Their dynamic is thus given by Equation (5.13) with

$$A_i^{\mathrm{SP}} = P_i, \text{ and } \; K_{i,i+N_g}^{\mathrm{SP}} = |E_i V_{i+N_g}/x_{\mathrm{d},i}|, i = 1, ..., N_g \tag{5.21}$$

and P_i the power produced by generator i. For loads and terminal nodes also Equation (5.13) is applied but with different parameters

$$H_i = 0, \quad A_i^{\mathrm{SP}} = -P_{l,i'} - |V_{i'}|^2 G_{ii}^{\mathrm{SP}}, \text{ and } \; K_{ij}^{\mathrm{SP}} = |V_{i'} V_{j'} Y_{ij}^{\mathrm{SP}}|, i = N_g + 1, ..., N_{\mathrm{n}} \; . \tag{5.22}$$

Thereby $i' = i - N_g$ denotes that the terminal nodes $i' = 1, ..., N_g$ have same power and voltage as the generator connected to it.

In this model the coupling matrix has the same topology (with additional internal nodes) as the physical network and is hence called structure preserving model. On the other hand it suffers the disadvantage that the dynamical D has to be estimated for the loads and terminal nodes.

Synchronous machines model (SM)

An alternative to the structure preserving model is to apply the full second order dynamic to the loads, too. Each node of the physical network is considered to be a terminal node with an internal node is attached it. We assume the former as passive and thus they are reduced by Kron-reduction. Therefore the network structure is not preserved during the calculation process. Nevertheless the information about the physical network is kept since the load internal nodes are dynamic and the state of the physical network can be reconstructed at any step of the calculation.

This model is identical with the EN model when the loads of the latter are considered as "generators producing negative power". The matrix $\mathbf{Y}_0'$ reads

$$\mathbf{Y}_0' = \left(\begin{array}{c|c} \mathbf{Y}_{\mathrm{d}} & -\mathbf{Y}_{\mathrm{d}} \\ \hline -\mathbf{Y}_{\mathrm{d}} & \mathbf{Y}_0 + \mathbf{Y}_{\mathrm{d}} \end{array} \right), \tag{5.23}$$

where $\mathbf{Y}_{\mathrm{d}}$ is a $N_{\mathrm{n}} \times N_{\mathrm{n}}$ matrix with the diagonal elements $Y_{\mathrm{d},jj} = (i\, x_{\mathrm{d},j})^{-1}$ and $\mathbf{Y}_0$ is the physical admittance matrix as derived in Section 5.1.

Kron-reduction of the terminal nodes of both generators and loads leads to a network of N_{n} coupled oscillators with the admittance matrix Y^{SM} that we can apply to Equation (5.13) with

$$A_i^{\mathrm{SM}} = +P_i - |E_i|^2 G_{ii}^{\mathrm{SM}} \quad \text{for generators,} \tag{5.24a}$$

$$A_i^{\mathrm{SM}} = -P_{l,i} - |E_i|^2 G_{ii}^{\mathrm{SM}} \quad \text{for loads and} \tag{5.24b}$$

$$K_{ij}^{\mathrm{SM}} = |E_i E_j Y_{ij}^{\mathrm{SM}}| \; . \tag{5.24c}$$

5.4. Stability of IEEE-50gen topology

In the previous Chapter 4 randomly created networks were investigated. Consequently the question arises if the results carry over to power grids, that exist in reality? Therefore in this section a power grid provided by the university of Washington[1] encoded in the IEEE format is investigated [18]. It is a test grid established with the aim to verify the accuracy of analytical techniques. First we address how to process these data and afterwards results of the stability measure are compared to those obtained using random networks.

The grid investigated in the following is the "50 Generator Dynamic Test Case" (or short "50-gen topology") [18]. It is stored in an ASCII-file containing two tables with their columns specified by the *IEEE common data format* that lists the raw data of every component as summarized in Table 5.1. For applying our simulation to this grid the coupling matrix K and hence $\mathbf{Y}_0$ is needed.

The package MATPOWER [7] provides a method "makeYbus.m" that implements the algorithm introduced in Section 5.1. As input it expects a Matlab object that basically contains the same column vectors as the IEEE data but in a slightly changed order.

With the matrix $\mathbf{Y}_0$ and the other parameters listed in Table 5.1 it is possible to calculate A and K for every of the three models introduced in Section 5.3. Since H, x_d and D are not given in this format, they have to be estimated. The damping D has been addressed in Section 2.7 and mainly reflects the (automatic) control mechanisms by the power grid governors. It turned out that $D = 50/\omega_\mathrm{r}$ p.u. is a good estimate [2]. Furthermore the inertia H and the transient reactance x_d of a synchronous machine are correlated to its power P [19]. We thus use $H = 0.04P$ (in seconds) and $x_\mathrm{d} = 92.8P^{-1.3}$ (in p.u.).

To obtain these parameters as well as K and D, it is also possible to use a Matlab script provided in the additional material of [2] whereby the Matlab format (mpc) is needed, see Table 5.1.

Exemplarily the SM model is applied to the 50-gen topology in the following. Processing the data as described above the coupling matrix K^SM, illustrated in Figure 5.4(a) is obtained. Moreover A and H are shown in Figure 5.4(b) and 5.4(c) respectively.

To compare the results of random networks with the specific 50-gen topology as well as homogeneous parameters with heterogeneous the basin stability (BS) approach is used again. Figure 5.5(a) shows the BS for the 50-gen topology with identical parameters chosen for every node $A_i = \pm 1$ depending on node i being generator or load, $H_i = 1$ and also for the lines $K_{ij} = 8\mathcal{A}_{ij}$. It is interesting to notice that the three peaked structure as observed in Section 4.2 also appears in this case while it in the latter different shape. The peak at $\mathcal{S}_\mathrm{B} \approx 0.2$ does not exist, only a few nodes have such a small stability. The peak at $\mathcal{S}_\mathrm{B} \approx 0.5$ can be identified but it has a significantly smaller magnitude while the peak at $\mathcal{S}_\mathrm{B} = 1$ has a larger one.

Since the number of connections to a node increases the stability, the higher average

[1] http://www2.ee.washington.edu/research/pstca/

raw data	Matpower input (mpc)	Matpower output	simulation parameters
R_s, X_s, B_c, τ	R_s, X_s, B_c, τ	$\mathbf{Y}_0$	K, ϕ
$P_g, P_l, Q_g, Q_l,$ P_S, Q_S	$P_g, P_l, Q_g, Q_l,$ P_S, Q_S	P, Q	A
		x_{d} (part of $\mathbf{Y}_0$, estimated)	
			D (estimated)
			H (estimated)
others			
defined by: IEEE case format	defined by: caseformat.m		defined: As described in text

Table 5.1.: From left to right the data given in the IEEE case format (definition also downloadable from the homepage of the university Washington) is rearranged to the mpc format (specification included as textfile in the Matpower package) then processed with Matpower and finally converted to the simulation parameters, as described in the text or by the additional material of[2]. P_g, Q_g are the active and reactive power generated by a generator, P_l, Q_l are the active and reactive power consumed by a load, P_S, Q_S are shunt losses and R_s, X_s are the real and imaginary part of the series impedance Z_s. The other quantities are as described during Chapter 5.

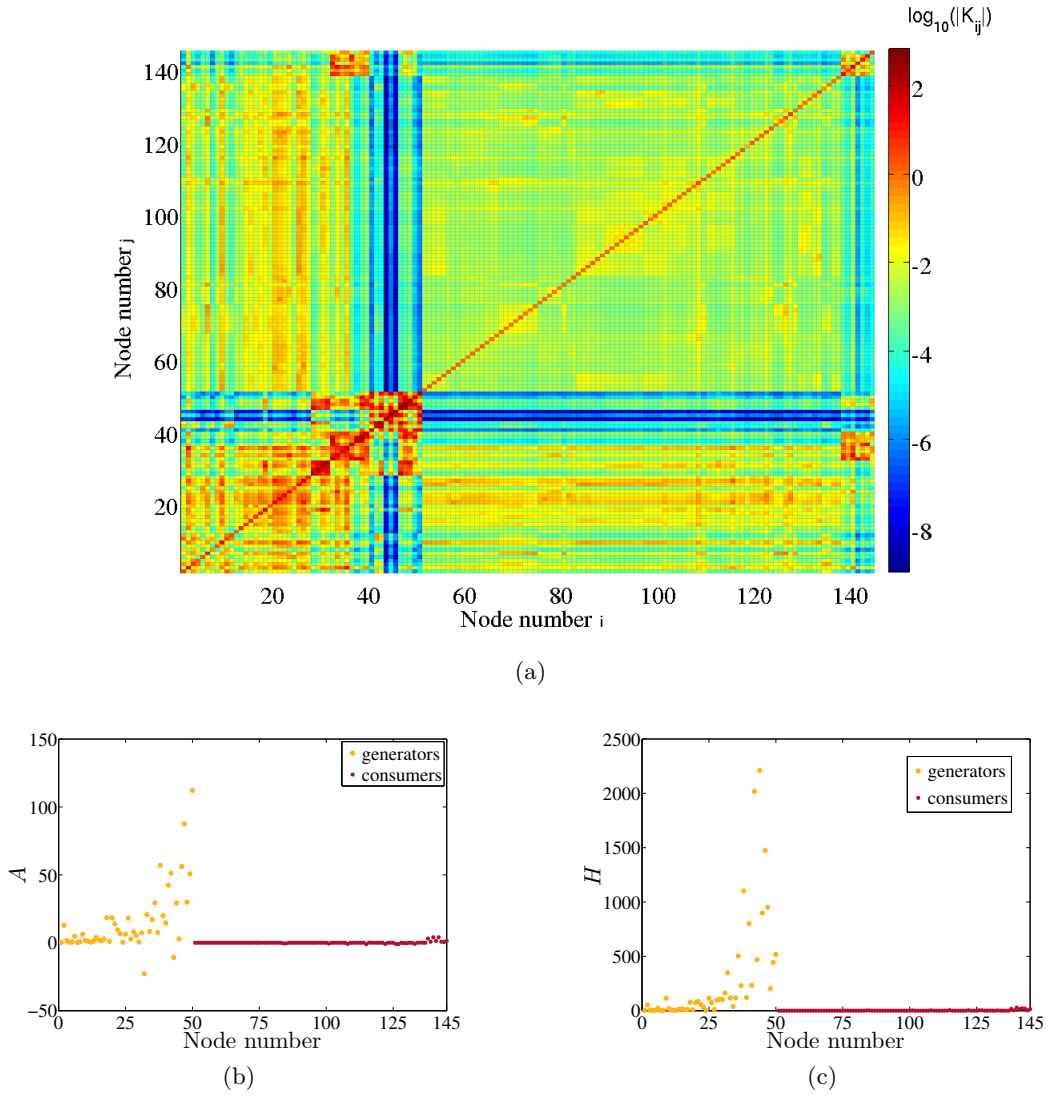

Figure 5.4.: Illustration of the simulation parameters of the 50-gen topology using the SM model. (a) Coupling matrix K_{ij} in a logarithmic scale with node i on x-axis and node j on y-axis. The diagonal elements are all zero since they are integrated in A. (b) Scaled power A. (c) Scaled inertia H. The nodes are re-indexed by 1 to 50 being generators and 51 to 145 being consumers in (a), (b) and (c).

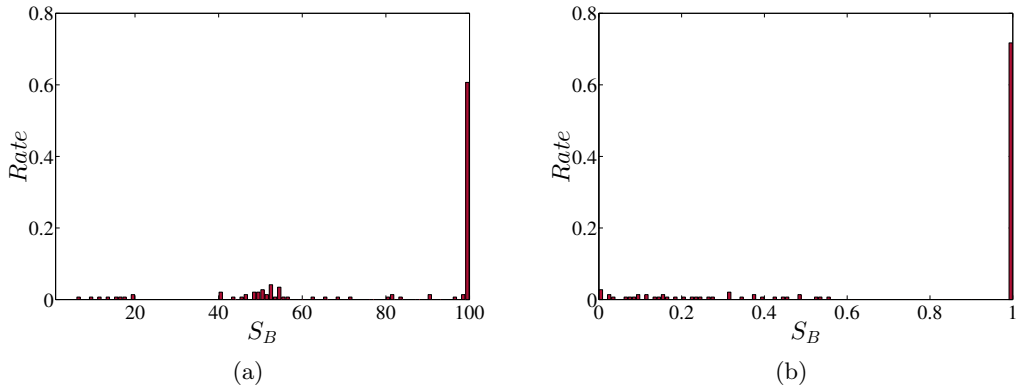

Figure 5.5.: Comparison of the distribution of BS in the 50-gen topology between (a) Identical parameters for each line and each node $K_{ij} = 8\mathcal{A}_{ij}$, $A_i = \pm 1$ (depending on node i being generator or consumer, randomly chosen) and $H = 1$ and (b) Parameters illustrated in Figure 5.4.

degree $\langle d \rangle = 1.52$ of the nodes in the 50-gen in comparison to that of the random networks $\langle d \rangle = 1.35$ is one argument. Another is that the grid is designed with less dead ends (11) than the average of the randomly created grids (≈ 19). To analyse this significantly change in the stability more systematically would be of interest for future publications.

If furthermore the heterogeneity in the parameters is applied to the grid, the stability distribution shown in Figure 5.5(b) is obtained. A three peaked structure is not visible. To get an insight into where these additional increase in the stability arises from, the BS is plotted for every node respectively in Figure 5.6.

It is noticeable that the stability for the loads is almost without an exception equal to one. Another conspicuous detail is the correlation between the magnitude of the parameters A, H and K with the stability $\mathcal{S}_\mathrm{B}$. This is meaningful since the perturbations of BS-method are not applied relatively but fixed. Therefore a frequency fluctuation at a generator producing a lot of power affects the grid stronger than the fluctuation at a load with relatively small demand. This emphasizes a study of various perturbations for instance the power fluctuation introduced in Section 3.3 on every node separately and observe the propagation of the perturbation though the network that is not done yet.

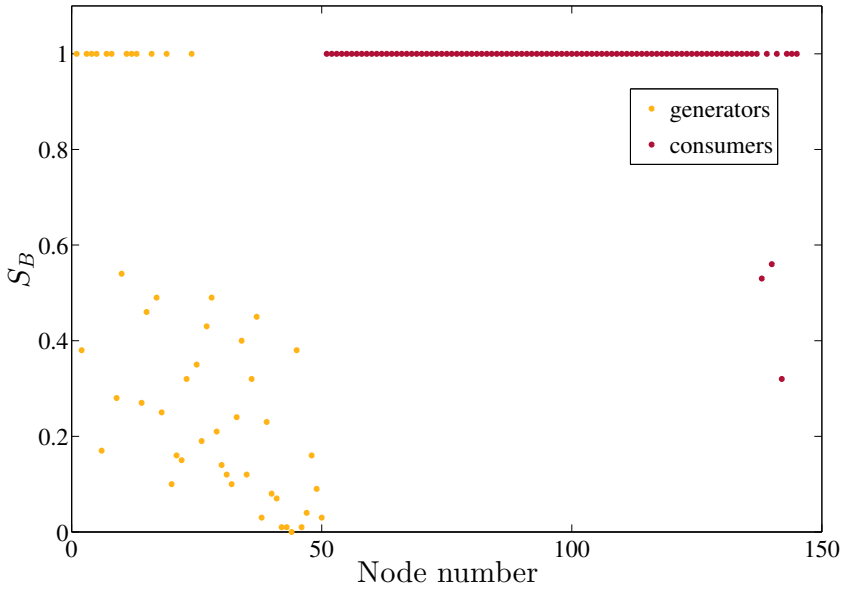

Figure 5.6.: Basin stability $\mathcal{S}_\mathrm{B}$ of the 50-gen grid with the original heterogeneous parameters plotted for every node separately. The nodes are re-indexed that 1-50 are generators and 51-145 are consumers.

6. Conclusion and Outlook

The dramatic increase of electrical energy production by renewable energy sources and the related simultaneously appearing decrease of conventional power plants comes along with new challenges for designing a reliable power grid. This motivates the investigation of power grids under different types of perturbations.

To realize this analysis we first addressed the basics of the power grids transmission lines and nodes that are mainly synchronous motors. In this context the different voltages levels were addressed as well as a brief introduction in the theoretical basis of networks, namely the Graph Theory. The description of the synchronous was done in two steps. First the physical principle and afterwards the mathematical were elucidated. Likewise a fundamental model of investigating synchronization, the Kuramoto model, was addressed.

To get familiar with the basin stability approach and the principles of simulating the dynamic of power grids the single node model was introduced. It consists of one generator (or load) with an effective coupling to a grid that is assumed to be of infinite size and therefore cannot be affected by the single nodes behaviour. Also a stochastic process was used to analyse the influence of a power fluctuation on the stability of the single node. The stochastic process was implemented such that it has some of the essential features of wind power. An open question is how this process would affect finite grids, were the interaction of the components is also dynamically simulated. Since the number of renewable energy power plants rises, it would also be interesting how the grid reacts on a growing number of nodes whose power generation follow this process.

A grid with a dynamic approach for every node has been investigated with basin stability. Properties of graphs and algorithms to create networks with specific properties were addressed. The distribution of the nodes stabilities and their correlations with the topology were studied by revisiting the work of Menck et al. [4].

Since it is not clear that random networks, even when created with suitable algorithms, reflect the behaviour of power grids existing in reality the topic of the last chapter was to compare a test system [18] with a grid having the same topology but the parameters used in the random grids. To achieve an accurate description of modelling power grids with realistic parameters of the components, different models were addressed [2] as well as packages[7] which provide parameter processing methods. It turned out that the heterogeneity, that was neglected within the study of the random networks, indeed has an influence of the stability distribution. In future publications a systematically study of the heterogeneity in the admittances and power production and demand would be insightful. Also the correlation with the grids topology has not been done yet. Here it was shown that the topology as well as the attributes of the components are designed to increase the stability of the grid im comparison to the ensemble of random grids. It has

be taken into account, that the synchronization in the 50-gen topology strongly depends on stable rotation of the generators and less on that of the loads.

A. Appendix

A.1. Example of Kron-reduction (Y-Δ transformation)

Here Y-Δ transformation, see Section 5.2, is demonstrated once with Gauss-elimination and another time with the algorithmic Kron-reduction formula.

The admittance matrix Y for the Y-network shown in Figure A.1 can be derived as described in Section 5.1. It reads

$$\mathbf{Y} = Y \begin{pmatrix} -1 & 0 & 0 & 1 \\ 0 & -1 & 0 & 1 \\ 0 & 0 & -1 & 1 \\ 1 & 1 & 1 & -3 \end{pmatrix} . \tag{A.1}$$

The unreduced current-balance equation therefore is

$$\left(\begin{array}{c} I_1 \\ I_2 \\ I_3 \\ \hline I_4 \end{array}\right) = Y \left(\begin{array}{ccc|c} -1 & 0 & 0 & 1 \\ 0 & -1 & 0 & 1 \\ 0 & 0 & -1 & 1 \\ \hline 1 & 1 & 1 & -3 \end{array}\right) \left(\begin{array}{c} V_1 \\ V_2 \\ V_3 \\ \hline V_4 \end{array}\right) . \tag{A.2}$$

We will now set the column vector of three ones at the top right side to zero by using **Gauss elimination**. A third of the fourth row is added to every other row and we obtain

$$\left(\begin{array}{c} I_1 + \frac{1}{3}I_4 \\ I_2 + \frac{1}{3}I_4 \\ I_3 + \frac{1}{3}I_4 \\ \hline I_4 \end{array}\right) = Y \left(\begin{array}{ccc|c} -\frac{2}{3} & \frac{1}{3} & \frac{1}{3} & 0 \\ \frac{1}{3} & -\frac{2}{3} & \frac{1}{3} & 0 \\ \frac{1}{3} & \frac{1}{3} & -\frac{2}{3} & 0 \\ \hline 1 & 1 & 1 & -3 \end{array}\right) \left(\begin{array}{c} V_1 \\ V_2 \\ V_3 \\ \hline V_4 \end{array}\right) . \tag{A.3}$$

Node 4 is a passive node meaning all current injected is also ejected

$$I_4 = \sum_j I_{4j} = 0 . \tag{A.4}$$

This leads to an equivalent relation only containing nodes one, two and three [17]

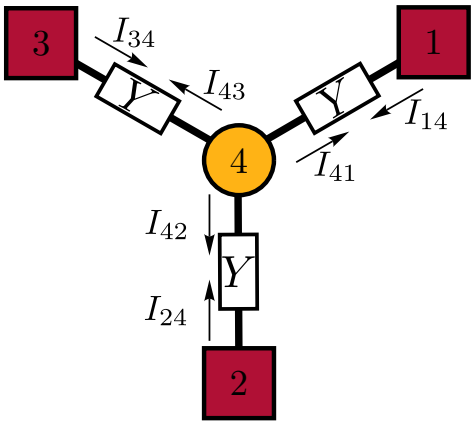

Figure A.1.: Network with admittances and currents, known as "Y-Network" due to the shape.

$$\begin{pmatrix} I_1 \\ I_2 \\ I_3 \end{pmatrix} = Y \begin{pmatrix} -\frac{2}{3} & \frac{1}{3} & \frac{1}{3} \\ \frac{1}{3} & -\frac{2}{3} & \frac{1}{3} \\ \frac{1}{3} & \frac{1}{3} & -\frac{2}{3} \end{pmatrix} \begin{pmatrix} V_1 \\ V_2 \\ V_3 \end{pmatrix} \quad . \tag{A.5}$$

The same result can be obtained by the **algorithmic formulation**

$$Y_{ij}^{\text{red}} = Y_{ij} - \frac{Y_{ik} Y_{kj}}{Y_{kk}}, \tag{A.6}$$

where k is the node that should be reduced, number four in this case. The Kron-reduction then reads

$$\begin{aligned}
Y_{11}^{\text{red}} &= Y_{11} - \frac{Y_{14}Y_{41}}{Y_{44}} = -1 - \frac{1 \cdot 1}{-3} = -\tfrac{2}{3}\,, \\
Y_{12}^{\text{red}} &= Y_{12} - \frac{Y_{14}Y_{42}}{Y_{44}} = 0 - \frac{1 \cdot 1}{-3} = \tfrac{1}{3}\,, \\
Y_{13}^{\text{red}} &= Y_{13} - \frac{Y_{14}Y_{43}}{Y_{44}} = 0 - \frac{1 \cdot 1}{-3} = \tfrac{1}{3}\,, \\
&\vdots \\
Y_{32}^{\text{red}} &= Y_{32} - \frac{Y_{34}Y_{42}}{Y_{44}} = 0 - \frac{1 \cdot 1}{-3} = \tfrac{1}{3} \text{ and} \\
Y_{33}^{\text{red}} &= Y_{33} - \frac{Y_{34}Y_{43}}{Y_{44}} = -1 - \frac{1 \cdot 1}{-3} = -\tfrac{2}{3}\,,
\end{aligned}$$

which yield the same Y^{red} as in equation A.5.

A.2. Example of admittance matrix creation

In this example we will derive the admittance matrix Y_0 for the power grid illustrated in figure A.2.

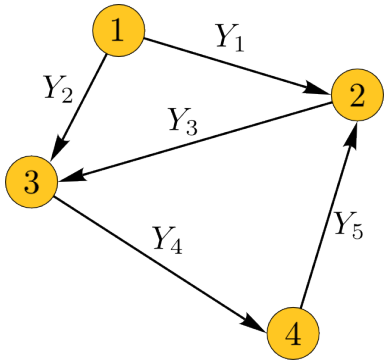

Figure A.2.: Power grid example with two generators, two loads and five branches.

At first we specify every branch with a number and its corresponding from- and to-node numbers as shown in table A.1.

branch	from-node	to-node
1	1	2
2	1	3
3	2	3
4	3	4
5	4	2

Table A.1.: Transmission lines with their corresponding from- and to-node indices.

Now we can express these connections in an other way with the connection matrices

$$C_\mathrm{f} = \begin{pmatrix} 1 & 0 & 0 & 0 \\ 1 & 0 & 0 & 0 \\ 0 & 1 & 0 & 0 \\ 0 & 0 & 1 & 0 \\ 0 & 0 & 0 & 1 \end{pmatrix} \qquad C_\mathrm{t} = \begin{pmatrix} 0 & 1 & 0 & 0 \\ 0 & 0 & 1 & 0 \\ 0 & 0 & 1 & 0 \\ 0 & 0 & 0 & 1 \\ 0 & 1 & 0 & 0 \end{pmatrix} \tag{A.7}$$

With these matrices from equation (A.7) we can calculate Y_f and Y_t

$$Y_\mathrm{f} = \begin{pmatrix} Y^1_\mathrm{ff} & Y^1_\mathrm{ft} & 0 & 0 \\ Y^2_\mathrm{ff} & 0 & Y^2_\mathrm{ft} & 0 \\ 0 & Y^3_\mathrm{ff} & Y^3_\mathrm{ft} & 0 \\ 0 & 0 & Y^4_\mathrm{ff} & Y^4_\mathrm{ft} \\ 0 & Y^5_\mathrm{ft} & 0 & Y^5_\mathrm{ff} \end{pmatrix} \qquad Y_\mathrm{t} = \begin{pmatrix} Y^1_\mathrm{tf} & Y^1_\mathrm{tt} & 0 & 0 \\ Y^2_\mathrm{tf} & 0 & Y^2_\mathrm{tt} & 0 \\ 0 & Y^3_\mathrm{tf} & Y^3_\mathrm{tt} & 0 \\ 0 & 0 & Y^4_\mathrm{tf} & Y^4_\mathrm{tt} \\ 0 & Y^5_\mathrm{tt} & 0 & Y^5_\mathrm{tf} \end{pmatrix} \tag{A.8}$$

and finally

$$Y_0 = \begin{pmatrix} [Y^1_{\mathrm{ff}} + Y^2_{\mathrm{ff}}] & Y^1_{\mathrm{ft}} & Y^2_{\mathrm{ft}} & 0 \\ Y^1_{\mathrm{tf}} & [Y^1_{\mathrm{tt}} + Y^3_{\mathrm{ff}} + Y^5_{\mathrm{tt}}] & Y^3_{\mathrm{ft}} & Y^5_{\mathrm{tf}} \\ Y^2_{\mathrm{tf}} & Y^3_{\mathrm{tf}} & [Y^2_{\mathrm{tt}} + Y^3_{\mathrm{tt}} + Y^4_{\mathrm{ff}}] & Y^4_{\mathrm{ft}} \\ 0 & Y^5_{\mathrm{ft}} & Y^4_{\mathrm{tf}} & [Y^4_{\mathrm{tt}} + Y^5_{\mathrm{ff}}] \end{pmatrix} + \mathbf{E}\vec{Y}_{\mathrm{shunt}} \quad \text{(A.9)}$$

Bibliography

[1] Erneuerbare energien 2015. http://nbn-resolving.de/urn:nbn:de:kobv:109-1-8330347, February 2016.

[2] T. Nishikawa and A. E. Motter. Comparative analysis of existing models for power-grid synchronization. *New Journal of Physics*, 2015.

[3] Klaus Heuck and Klaus-Dieter Dettmann. *Elektrische Energieversorgung*. Vieweg, 2 edition, 1991. german.

[4] P. J. Menck, J. Heitzig, J. Kurths, and H. J. Schellnhuber. How dead ends undermine power grid stability. *nature communications*, 2014.

[5] Pedro G Lind. The network approach: basic concepts and algorithms. arXiv, November 2007.

[6] B. la Bollobás, O. Riordan, and A. Barabási et al. *Handbook of Graphs and Networks*. Wiley-VCH, 2005.

[7] Ray D. Zimmerman and Carlos E. Murillo-Sánchez. *Matpower User's Manual*. Cornell University, 6.0b1 edition, June 2016.

[8] Yoshiki Kuramoto. *International Symposium on Mathematical Problems in Theoretical Physics*, volume 39, chapter Self-entrainment of a population of coupled non-linear oscillators, pages 420–422. Springer, January 1975. ISBN: 978-3-540-07174-7 (Print) 978-3-540-37509-8 (Online).

[9] Katrin Schmietendorf. Synchronisation und spannungsstabilität in einem netzwerk von synchronmaschinen. Master's thesis, Westfälische Wilhelms-Universität Münster, July 2012. (german).

[10] Continental europe operation handbook. https://www.entsoe.eu/publications/system-operations-reports/operation-handbook/Pages/default.aspx, June 2004. Appendix A1.

[11] C. Grigg et al. The ieee reliability test system -1996. *IEEE Transactions on Power System*, 14(3):1010–1020, August 1999.

[12] Peter Johannes Menck. *How Wires Shape Volumes*. PhD thesis, Humboldt-Universität zu Berlin, Oktober 2013.

[13] Patrick Milan, Matthias Wächter, and Joachim Peinke. Stochastic modeling and performance monitoring of wind farm power production. *J. Renewable Sustainable Energy*, 6, May 2014.

[14] G. A. M. van Kuik, J. Peinke, and et al. Long-term research challenges in wind energy - a research agenda by the european academy of wind energy. *Wind Energy Science*, pages 1–39, 2016.

[15] Ducan J Watts and Steven H Strogaz. Collective dynamics of 'small-world' networks. *Nature*, 393:440–442, June 1998.

[16] Erdös and Rényi. *Publ. Math. (Debrecen)*, 6:290, 1959.

[17] Florian Dörfler and Fransesco Bullo. Kron reduction of graphs with applications to electrical networks. *IEEE Transactions on Circuits and Systems I: Regular Papers*, 60:150–163, January 2013.

[18] V. Vittal. ransient stability test systems for direct stability methods. *IEEE T. Power Syst.*, 7:37–43, 1992.

[19] Adilson E. Motter and Takashi Nishikawa. Spontaneous synchrony in power-grid networks. *Nature Physics*, 9:191–197, 2013.